Multiple-Step Kinetic Mechanisms of the ssDNA Recognition Process by Human Polymerase β in Its Different ssDNA Binding Modes[†]

Surendran Rajendran, Maria J. Jezewska, and Wlodzimierz Bujalowski*

Department of Human Biological Chemistry and Genetics, Sealy Center for Structural Biology, The University of Texas Medical Branch at Galveston, 301 University Boulevard, Galveston, Texas 77555-1053

Received June 6, 2001; Revised Manuscript Received July 18, 2001

ABSTRACT: The kinetics of human polymerase β (pol β) binding to the single-stranded DNA, in the (pol β)$_{16}$ and (pol β)$_5$ binding modes, that differ in the number of occluded nucleotide residues in the protein−DNA complexes, have been examined, using the fluorescence stopped-flow technique. This is the first determination of the mechanism of ssDNA recognition by human pol β. Binding of the enzyme to the ssDNA containing fluorescein in the place of one of the nucleotides is characterized by a strong DNA fluorescence increase, providing the required signal to quantitatively examine the complex mechanism of ssDNA recognition. The experiments were performed with the ssDNA 20-mer, which engages the polymerase in the (pol β)$_{16}$ binding mode and encompasses the total DNA-binding site of the enzyme, and with the 10-mer, which exclusively forms the (pol β)$_5$ binding mode engaging only the 8-kDa domain of the enzyme. The obtained data and analyses indicate that the (pol β)$_{16}$ formation occurs by a minimum four-step, sequential mechanism:

$$\text{Human pol}\beta + \text{ssDNA} \underset{k_{-1}}{\overset{k_1}{\leftrightarrow}} (P_{16}\text{-ssDNA})_1 \underset{k_{-2}}{\overset{k_2}{\leftrightarrow}} (P_{16}\text{-ssDNA})_2 \underset{k_{-3}}{\overset{k_3}{\leftrightarrow}} (P_{16}\text{-ssDNA})_3 \underset{k_{-4}}{\overset{k_4}{\leftrightarrow}} (P_{16}\text{-ssDNA})_4$$

Formation of the (pol β)$_5$ binding mode proceeds with the same mechanism; however, both binding modes differ in the energetics of the partial reactions and the structure of the intermediates. Quantitative amplitude analysis, using the matrix projection operator approach, allowed us to determine molar fluorescence intensities of all intermediates relative to the fluorescence of the free DNA. The results indicate that (pol β)$_{16}$ binding mode formation, which is initiated by the association of the 8-kDa domain with the DNA, is followed by subsequent intermediates stabilized by DNA binding to the 31-kDa domain. Comparison with the (pol β)$_5$ binding mode formation indicates that transitions of the enzyme−DNA complex in both modes are induced at the interface of the 8-kDa domain and the DNA. The sequential nature of the mechanism indicates the lack of a conformational preequilibrium of the enzyme prior to ssDNA binding.

Polymerase β is one of a number of recognized DNA-directed polymerases of the eukaryotic nucleus (*1*−*5*). A characteristic feature of human pol β[1] is a "simplified" set of activities. The enzyme lacks intrinsic accessory activities, such as 3′ or 5′ exonuclease, endonuclease, dNMP turnover, and pyrophosphorolysis (*1*, *6*−*8*). This limited repertoire of activities reflects the very specialized function of the enzyme in human cell repair machinery, which includes the gap-filling synthesis involved in mismatch repair and the repair of monofunctional adducts, UV-damaged DNA, and abasic lesions in DNA (*9*−*14*).

The crystal structure of human pol β revealed a typical polymerase fold, a thumb, palm, and fingers, due to its resemblance to the human hand (*15*−*18*). The feature that distinguishes the pol β structure from other polymerases is the presence of a small 8-kDa domain connected with the tip of the fingers through a tether of 14 amino acids (*15*−*17*). The domain possesses the ability to catalyze the release of the 5′-terminal deoxyribose phosphate residue from the incised apurinic-apirimidinic site that is a common intermediate product in base excision repair (*8*). Although it is well established that the active site of DNA synthesis resides in the large 31-kDa catalytic domain, the role of both domains in the recognition of the DNA substrates is only now emerging (*19*−*23*).

Quantitative thermodynamic data have shown that both human and rat pol β bind the ssDNA in two binding modes which differ in the number of occluded nucleotide residues, the (pol β)$_{16}$ and (pol β)$_5$ binding modes (*19*−*23*). Both binding modes differ in affinities and abilities to induce conformational changes in the nucleic acid (*20*). Thus, the intrinsic affinity of the enzyme in the (pol β)$_{16}$ binding mode is approximately an order of magnitude higher than the affinity in the (pol β)$_5$ binding mode. However, the enzyme induces much more profound structural changes in the ssDNA, when bound in the (pol β)$_5$ binding mode, indicating strong base−base separation and immobilization in the complex. In the (pol β)$_{16}$ binding mode, both the 8- and 31-kDa domains of

[†] This work was supported by NIH Grant GM-58565 (to W.B.).

* Address correspondence to this author at the Department of Human Biological Chemistry and Genetics, The University of Texas Medical Branch at Galveston, 301 University Blvd., Galveston, TX 77555-1053. Tel: (409) 772-5643; Fax: (409) 772-1790; Email: wbujalow@utmb.edu.

[1] Abbreviations: pol β, polymerase β; ssDNA, single-stranded DNA; dsDNA, double-stranded DNA.

10.1021/bi011173j CCC: $20.00
Published on Web 09/06/2001

the enzyme are involved in interactions with the ssDNA, while in the (pol β)$_5$ binding mode, the 8-kDa domain is predominantly engaged in interactions with the DNA (*20*).

Recent analysis has shown that the 8-kDa domain of rat pol β has both ssDNA and dsDNA affinity of similar magnitude (*21*). This ability of the DNA-binding site, located on the 8-kDa domain, to interact with different nucleic acid conformations appears to be crucial for anchoring the enzyme at the template-primer and gapped-DNA substrates (*21*−*23*). The DNA-binding site of the domain has an energetically homogeneous structure allowing the domain to accommodate DNA oligomers of different lengths with similar affinity. These data also indicate that the site-size and affinity of the DNA-binding site located on the 8-kDa domain are specifically controlled by the binding of magnesium cations to the domain (*21*). The results of the equilibrium studies clearly show that the total DNA-binding site of pol β is built of two DNA-binding subsites, each capable of interacting with different conformations of the DNA and responding differently to the presence of salt and divalent cations in solution.

Elucidation of the human pol β−ssDNA recognition processes constitutes the first step toward understanding the activities of the polymerase at the molecular level. Despite the paramount importance for understanding the polymerase mechanism, the direct analysis of the kinetics of ssDNA recognition by human pol β so far has not been quantitatively addressed.

In this paper, we report the kinetic analyses of human pol β interactions with the ssDNA in the (pol β)$_{16}$ and (pol β)$_5$ binding modes, using the fluorescence stopped-flow technique. The quantitative analysis of the kinetic data was performed using the matrix projection operator approach (*24*−*26*). We provide direct evidence that the mechanism of (pol β)$_{16}$ binding mode formation by the enzyme is a four-step, sequential reaction. The binding is initiated by the 8-kDa domain association with the DNA followed by subsequent intermediates, stabilized by DNA binding to the DNA-binding subsite located on the 31-kDa domain. Formation of the (pol β)$_5$ binding mode proceeds with the same general mechanism; however, both binding modes differ in the stability and structure of the intermediates. The data indicate that the conformational transitions of the enzyme−ssDNA complexes are induced by interactions between the ssDNA-binding subsite located on the small 8-kDa domain and the nucleic acid in both binding modes.

MATERIALS AND METHODS

Reagents and Buffers. All solutions were made with distilled and deionized >18 MΩ (Milli-Q Plus) water. All chemicals were reagent grade. Buffer C is 10 mM sodium cacodylate adjusted to pH 7.0 with HCl, 10% glycerol. The temperatures and concentrations of the NaCl and $MgCl_2$ in the buffer are indicated in the text.

Human Polymerase β. Human pol β was purified using a previously published procedure (*27, 28*). The concentrations of the protein were determined using the extinction coefficient $\epsilon_{280} = 2.1 \times 10^4$ cm^{-1} M^{-1} determined by the approach based on the Edelhoch method (*28*−*30*).

Nucleic Acids. Oligomers, dT(pT)$_8$-pFlu-(pT)$_{10}$, dT(pT)$_{15}$-pFlu-(pT)$_4$, dT(pT)$_3$-pFlu-(pT)$_5$, and dA(pA)$_8$-pFlu-(pA)$_{10}$, were purchased from Midland Certified Reagents (Midland, TX). Oligomers were at least >95% as judged by autoradiography on polyacrylamide gels. The fluorescein residue is introduced through the fluorescein phosphoramidate; i.e., the label replaces one of the bases in the oligomers. The nucleic acid concentrations were determined as previously described by us (*31*−*33*).

Fluorescence Measurements. Steady-state fluorescence titrations were performed using the SLM-AMINCO 8100 spectrofluorometer. To avoid possible artifacts, due to the fluorescence anisotropy of the sample, polarizers were placed in excitation and emission channels and set at 90° and 55° (magic angle), respectively (*31*−*34*). The fractional fluorescence increase of the nucleic acids is defined as $\Delta F = (F_i - F_o)/F_o$ where F_i is the value of the fluorescence intensity at a given titration point and F_o is the initial fluorescence intensity of the sample (*34*).

Stopped-Flow Kinetics. All fluorescence stopped-flow kinetic experiments were performed using the SX.MV18 sequential stopped-flow instrument (Applied Photophysics Ltd., Leatherhead, U.K.). The instrument has a dead-time of ∼1.5 ms. The reactions were monitored using the fluorescence of the ssDNA oligomers, containing the fluorescein residue, with $\lambda_{ex} = 485$ nm, and emission was observed through a GG495 cutoff filter (Schott, PA), with the excitation monochromator slits at 1.5 mm (band-pass ∼6.5 nm). A total of 4000 points were collected in each trace that also contained a steady-state value of the sample fluorescence recorded 2 ms before the flow stops. Usually, 8−15 traces were collected and averaged for each sample. The kinetic curves were fitted to extract relaxation times and amplitudes using nonlinear least-squares software provided by the manufacturer, with the exponential function defined as

$$F(t) = F(\infty) + \sum_{i=1}^{n} A_i \exp(-\lambda_i t) \qquad (1)$$

where $F(t)$ is the fluorescence intensity at time t, $F(\infty)$ is the fluorescence intensity at $t = \infty$, A_i is the amplitude corresponding to the ith relaxation process, λ_i is the time constant (reciprocal relaxation time) characterizing the ith relaxation process, and n is the number of relaxation processes. All further analyses of the data were performed using Mathematica (Wolfram, Urbana, IL) and Kaleida Graph (Synergy Software, PA) on Macintosh G3 or G4 computers.

THEORY

Analysis of Stopped-Flow Kinetic Data. Application of the Matrix Projection Operator Technique. Examination of both the relaxation times and the amplitudes of the observed normal modes of the reaction is crucial for the quantitative determination of the mechanism of macromolecule−ligand interactions, using spectroscopic measurements (*24, 25, 35*−*37*). The rate constants characterizing particular steps are mainly obtained from the examination of the relaxation times of the system. However, the amplitude analysis can prove or disprove the determined mechanism and, moreover, can provide information about the structure of the intermediates (*24, 25, 35*−*37*). The analysis is greatly facilitated if relaxation times and amplitudes of all normal modes of the reaction are determined from the experiment. On the other hand, a common situation in stopped-flow studies of the

binding system is that the relaxation time characterizing the bimolecular step is too fast to be accessed in the examined time range longer than the dead-time of the instrument, i.e., $t > \sim 1-2$ ms. However, as discussed below, in such cases the rate constants of the binding step and the spectroscopic parameter characterizing the first intermediate can still be determined from the analysis of amplitudes, particularly the amplitude of the first normal mode of the reaction.

The data described in this work show that the dynamics of human pol β binding to the ssDNA in both the (pol β)$_{16}$ and (pol β)$_5$ binding modes include the bimolecular step leading to the formation of the initial complex, which subsequently undergoes several first-order conformational transitions. This is a sequential reaction between nucleic acid (macromolecule), N_1, and polymerase (ligand), C, described by eq 2:

$$C + N_1 \underset{k_{-1}}{\overset{k_1}{\rightleftharpoons}} N_2 \underset{k_{-2}}{\overset{k_2}{\rightleftharpoons}} N_3 \underset{k_{-3}}{\overset{k_3}{\rightleftharpoons}} N_4 \underset{k_{-4}}{\overset{k_4}{\rightleftharpoons}} N_5 \qquad (2)$$

The reaction is monitored by the fluorescence change of the macromolecule. The differential equations describing the time course of reaction 2, in terms of different macromolecule species, are

$$\frac{dN_1}{dt} = -k_1N_1C + k_{-1}N_2 \qquad (3a)$$

$$\frac{dN_2}{dt} = k_1N_1C - (k_{-1} + k_2)N_2 + k_{-2}N_3 \qquad (3b)$$

$$\frac{dN_3}{dt} = k_2N_2 - (k_{-2} + k_3)N_3 + k_{-3}N_4 \qquad (3c)$$

$$\frac{dN_4}{dt} = k_3N_3 - (k_{-3} + k_4)N_4 + k_{-4}N_5 \qquad (3d)$$

$$\frac{dN_5}{dt} = k_4N_4 - k_{-4}N_5 \qquad (3e)$$

Kinetic studies described in this work have been performed under pseudo-first-order conditions with large excess of the enzyme over the nucleic acid, $C_{tot} \gg N_{tot}$; i.e., C_{tot} is approximately constant during the reaction. In matrix notation, system 3 is then defined as

$$\begin{pmatrix} \frac{dN_1}{dt} \\ \frac{dN_2}{dt} \\ \frac{dN_3}{dt} \\ \frac{dN_4}{dt} \\ \frac{dN_5}{dt} \end{pmatrix} = \begin{pmatrix} -k_1C & k_{-1} & 0 & 0 & 0 \\ k_1C & -(k_{-1}+k_2) & k_{-2} & 0 & 0 \\ 0 & k_2 & -(k_{-2}+k_3) & k_{-3} & 0 \\ 0 & 0 & k_3 & -(k_{-3}+k_4) & k_{-4} \\ 0 & 0 & 0 & k_4 & -k_{-4} \end{pmatrix} \begin{pmatrix} N_1 \\ N_2 \\ N_3 \\ N_4 \\ N_5 \end{pmatrix} \qquad (4)$$

and

$$\dot{\mathbf{N}} = \mathbf{M}\mathbf{N} \qquad (5)$$

where $\dot{\mathbf{N}}$ is a vector of time derivatives, **M** is the coefficient matrix, and **N** is the vector of concentrations of different nucleic acid forms in solution. In the standard matrix approach, the solution of system 4 is

$$\mathbf{N} = \exp(\mathbf{M}t)\mathbf{N}_0 \qquad (6)$$

where

$$\exp(\mathbf{M}t) = \mathbf{V}\begin{bmatrix} \exp(\lambda_0 t) & 0 & 0 & 0 & 0 \\ 0 & \exp(\lambda_1 t) & 0 & 0 & 0 \\ 0 & 0 & \exp(\lambda_2 t) & 0 & 0 \\ 0 & 0 & 0 & \exp(\lambda_3 t) & 0 \\ 0 & 0 & 0 & 0 & \exp(\lambda_4 t) \end{bmatrix}\mathbf{V}^{-1} \qquad (7)$$

Quantities λ_0, λ_1, λ_2, λ_3, and λ_4 are eigenvalues of matrix **M**, **V** is a matrix whose columns are the eigenvectors of matrix **M**, and $\mathbf{N_0}$ is the vector of the initial concentrations. In the considered case, $\mathbf{N_0}$ is a column vector (N_{tot}, 0, 0, 0, 0), where N_{tot} is the total concentration of the nucleic acid (macromolecule). However, to obtain closed-form expressions for amplitudes of the reaction that are most suitable for the quantitative analysis of the intermediates, we expand matrix exp(**M***t*) using its eigenvalues, exp($\lambda_i t$), and the corresponding projection operators, $\mathbf{Q_i}$, as (*24*, *25*, *38*)

$$\exp(\mathbf{M}t) = \sum_{i=0}^{4} \mathbf{Q_i} \exp(\lambda_i t) \qquad (8)$$

The projection operators, $\mathbf{Q_i}$, are analytically defined using the original coefficient matrix **M** and its eigenvalues, λ_i (*24*, *25*). A general formula for a projection operator, $\mathbf{Q_i}$, corresponding to an eigenvalue, λ_i, is (*24*, *25*, *38*)

$$\mathbf{Q_i} = \frac{\prod_{j \neq i}^{n} (\mathbf{M} - \lambda_j \mathbf{I})}{\prod_{j \neq i}^{n} (\lambda_i - \lambda_j)} \qquad (9)$$

where *n* is the number of eigenvalues.

In the considered case, there are five eigenvalues: λ_0, λ_1, λ_2, λ_3, and λ_4. One eigenvalue, $\lambda_0 = 0$, is the result of the mass conservation in the reaction system (*24*, *25*). The solution for the examined system of differential equations, expressed in terms of matrix projection operators, is

$$\mathbf{N} = \mathbf{Q_0N_0} + \mathbf{Q_1N_0} \exp(\lambda_1 t) + \mathbf{Q_2N_0} \exp(\lambda_2 t) + \mathbf{Q_3N_0} \exp(\lambda_3 t) + \mathbf{Q_4N_0} \exp(\lambda_4 t) \qquad (10)$$

where $\mathbf{Q_i}$ are defined by eq 9.

Because the projection operators, $\mathbf{Q_i}$, are matrices of the same size as the size of the original coefficient matrix **M**, the products $\mathbf{Q_iN_0}$ are column vectors, $\mathbf{P}_i$, which are the projections of $\mathbf{N_0}$ on each eigenvector of matrix **M**. The solution of the differential equation system 3 is then

$$\mathbf{N} = \mathbf{P_0} + \mathbf{P_1}\exp(\lambda_1 t) + \mathbf{P_2}\exp(\lambda_2 t) + \mathbf{P_3}\exp(\lambda_3 t) + \mathbf{P_4}\exp(\lambda_4 t) \quad (11a)$$

and

$$\begin{pmatrix} N_1 \\ N_2 \\ N_3 \\ N_4 \\ N_5 \end{pmatrix} = \begin{pmatrix} P_{01} \\ P_{02} \\ P_{03} \\ P_{04} \\ P_{05} \end{pmatrix} + \begin{pmatrix} P_{11} \\ P_{12} \\ P_{13} \\ P_{14} \\ P_{15} \end{pmatrix}\exp(\lambda_1 t) + \begin{pmatrix} P_{21} \\ P_{22} \\ P_{23} \\ P_{24} \\ P_{25} \end{pmatrix}\exp(\lambda_2 t) + \begin{pmatrix} P_{31} \\ P_{32} \\ P_{33} \\ P_{34} \\ P_{35} \end{pmatrix}\exp(\lambda_3 t) + \begin{pmatrix} P_{41} \\ P_{42} \\ P_{43} \\ P_{44} \\ P_{45} \end{pmatrix}\exp(\lambda_4 t) \quad (11b)$$

where P_{ij} is the jth element of the projection of the vector of the initial concentrations of $\mathbf{N_0}$ on the eigenvector corresponding to the ith eigenvalue of the matrix $\mathbf{M}$.

In the considered mechanism defined by eq 2, the four normal modes of the reaction have relaxation times $\tau_1 = -1/\lambda_1$, $\tau_2 = -1/\lambda_2$, $\tau_3 = -1/\lambda_3$, and $\tau_4 = -1/\lambda_4$ and four corresponding individual amplitudes, A_1, A_2, A_3, and A_4. Each individual amplitude contains a contribution from the fluorescence intensities characterizing all intermediates of the reaction. In a general case, each intermediate may have different fluorescence properties. Therefore, there are five molar fluorescence intensities, F_1, F_2, F_3, F_4, and F_5, characterizing the N_1, N_2, N_3, N_4, and N_5 states of the macromolecule, free and in the complexes with the ligand. The total concentration of the macromolecule during the reaction obeys the mass conservation relationship

$$N_{tot} = N_1 + N_2 + N_3 + N_4 + N_5 \quad (12)$$

Therefore, at any time of the reaction, the fluorescence of the system, $F(t)$, is defined as

$$F(t) = F_1N_1 + F_2N_2 + F_3N_3 + F_4N_4 + F_5N_5 \quad (13)$$

Introducing eqs 11b and 12 into eq 13 and rearranging provides

$$F(t) = F_1N_1 + \begin{pmatrix} F_2P_{02} + F_3P_{03} + F_4P_{04} + F_5P_{05} \\ F_2P_{12} + F_3P_{13} + F_4P_{14} + F_5P_{15} \\ F_2P_{22} + F_3P_{23} + F_4P_{24} + F_5P_{25} \\ F_2P_{32} + F_3P_{33} + F_4P_{34} + F_5P_{35} \\ F2P_{42} + F_3P_{43} + F_4P_{44} + F_5P_{45} \end{pmatrix}^T \begin{pmatrix} 1 \\ \exp(\lambda_1 t) \\ \exp(\lambda_2 t) \\ \exp(\lambda_3 t) \\ \exp(\lambda_4 t) \end{pmatrix} \quad (14)$$

where index T indicates the transpose vector. The experimentally determined total amplitude, A_{tot}, of a stopped-flow trace is defined as (*24*, *25*)

$$A_{tot} = F(\infty) - F(0) \quad (15)$$

where $F(0)$ and $F(\infty)$ are the observed fluorescence intensities, $F(t)$, of the system at $t = 0$ and $t = 8$, respectively. Introducing $t = 0$ for $F(0)$ and $t = \infty$ for $F(\infty)$ into eq 14 provides

$$F(0) = F_1N_{tot} + \begin{pmatrix} P_{02} + P_{12} + P_{22} + P_{32} + P_{42} \\ P_{03} + P_{13} + P_{23} + P_{33} + P_{43} \\ P_{04} + P_{14} + P_{24} + P_{34} + P_{44} \\ P_{05} + P_{15} + P_{25} + P_{35} + P_{45} \end{pmatrix}^T \begin{pmatrix} F_1 - F_2 \\ F_1 - F_3 \\ F_1 - F_4 \\ F_1 - F_5 \end{pmatrix} \quad (16a)$$

and

$$F(\infty) = F_1N_{tot} + (P_{02}P_{03}P_{04}P_{05}) \begin{pmatrix} F_1 - F_2 \\ F_1 - F_3 \\ F_1 - F_4 \\ F1 - F_5 \end{pmatrix} \quad (16b)$$

Subtracting eq 16a from 16b gives the total amplitude as

$$A_{tot} = \begin{pmatrix} P_{12} + P_{13} + P_{14} + P_{15} \\ P_{22} + P_{23} + P_{24} + P_{25} \\ P_{32} + P_{33} + P_{34} + P_{35} \\ P_{42} + P_{43} + P_{44} + P_{45} \end{pmatrix}^T \begin{pmatrix} F_1 - F_2 \\ F_1 - F_3 \\ F_1 - F_4 \\ F_1 - F_5 \end{pmatrix} \quad (17)$$

Because the total amplitude, A_{tot}, of the stopped-flow trace is the sum of the individual amplitudes of all normal modes

$$A_{tot} = A_1 + A_2 + A_3 + A_4 \quad (18)$$

The individual amplitudes A_1, A_2, A_3, and A_4 for each normal mode of the reaction are then

$$A_1 = (P_{12}\ P_{13}\ P_{14}\ P_{15}) \begin{pmatrix} F_1 - F_2 \\ F_1 - F_3 \\ F_1 - F_4 \\ F_1 - F_5 \end{pmatrix} \quad (19a)$$

$$A_2 = (P_{22}\ P_{23}\ P_{24}\ P_{25}) \begin{pmatrix} F_1 - F_2 \\ F_1 - F_3 \\ F_1 - F_4 \\ F_1 - F_5 \end{pmatrix} \quad (19b)$$

$$A_3 = (P_{32}\ P_{33}\ P_{34}\ P_{35}) \begin{pmatrix} F_1 - F_2 \\ F_1 - F_3 \\ F_1 - F_4 \\ F_1 - F_5 \end{pmatrix} \quad (19c)$$

$$A_4 = (P_{42}\ P_{43}\ P_{44}\ P_{45}) \begin{pmatrix} F_1 - F_2 \\ F_1 - F_3 \\ F_1 - F_4 \\ F_1 - F_5 \end{pmatrix} \quad (19d)$$

Equations 19a−d are closed-form, explicit expressions for the individual amplitudes for the four-step reaction mechanism described by eq 2 (*24*, *25*). In other words, once the matrix projection operators are formulated in terms of the original matrix of coefficients $\mathbf{M}$, the total and individual amplitudes of the reaction system can be defined in terms of rate constants, relaxation times, and spectroscopic properties of the intermediates.

Relaxation Times. The examination of the relaxation times of the studied stopped-flow kinetics, as a function of the ligand concentration, is the first and fundamental step in establishing the mechanism of a complex reaction and determining the rate constants of particular elementary processes (*24*). The reciprocal relaxation times for the four-step sequential reaction, described by eq 2, as a function of

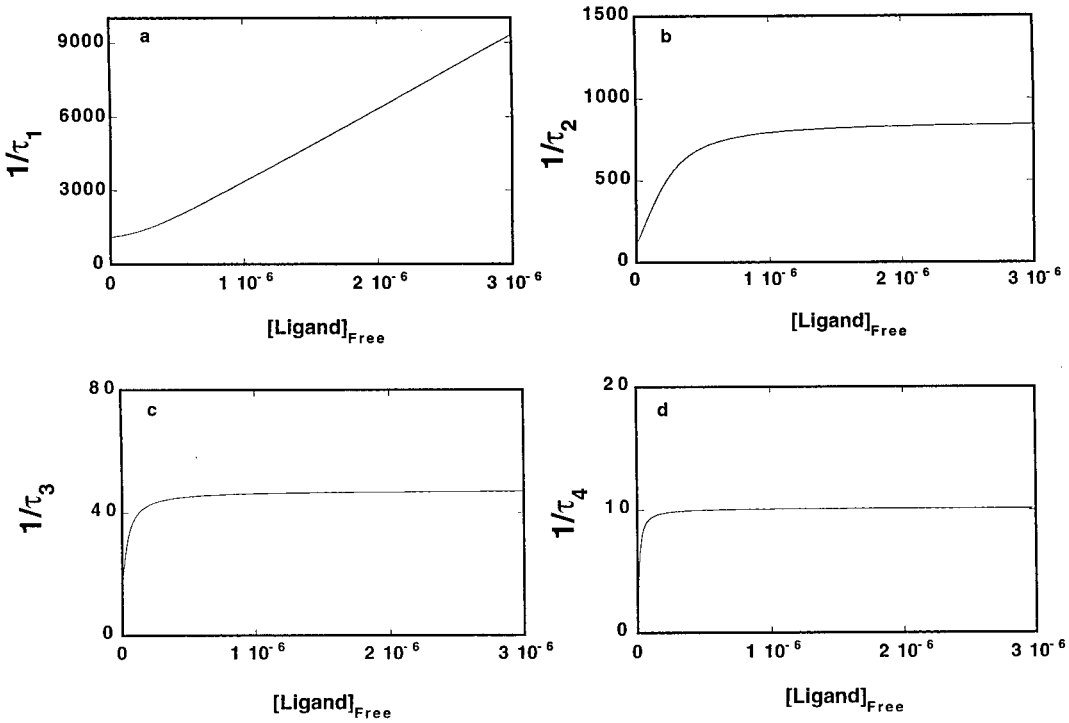

FIGURE 1: Computer simulation of the dependence of reciprocal relaxation times (s^{-1}) for the four-step sequential mechanism of ligand binding to a macromolecule, defined by eq 2, upon the free ligand concentration. Relaxation times have been obtained by numerically determining the eigenvalues of the matrix of coefficient **M** (λ_1, λ_2, λ_3, λ_4) and using identities: $1/\tau_1 = -\lambda_1$, $1/\tau_2 = -\lambda_2$, $1/\tau_3 = -\lambda_3$, and $1/\tau_4 = -\lambda_4$. The simulations have been performed using rate constants: $k_1 = 3 \times 10^9$ M^{-1} s^{-1}, $k_{-1} = 300$ s^{-1}, $k_2 = 600$ s^{-1}, $k_{-2} = 250$ s^{-1}, $k_3 = 50$ s^{-1}, $k_{-3} = 10$ s^{-1}, $k_4 = 10$ s^{-1}, and $k_{-4} = 3$ s^{-1}. (a) $1/\tau_1$, (b) $1/\tau_2$, (c) $1/\tau_3$, (d) $1/\tau_4$.

the free ligand concentration are shown in Figure 1a−d. Relaxation times have been obtained by direct, numerical determination of the eigenvalues, λ_1, λ_2, λ_3, and λ_4, of the matrix **M**, at a given free ligand concentration, C_1, using the identities of $1/\tau_1 = -\lambda_1$, $1/\tau_2 = -\lambda_2$, $1/\tau_3 = -\lambda_3$, and $1/\tau_4 = -\lambda_4$. The selected rate constants are as follows: $k_1 = 3 \times 10^9$ M^{-1} s^{-1}, $k_{-1} = 300$ s^{-1}, $k_2 = 600$ s^{-1}, $k_{-2} = 250$ s^{-1}, $k_3 = 50$ s^{-1}, $k_{-3} = 10$ s^{-1}, $k_4 = 10$ s^{-1}, and $k_{-4} = 3$ s^{-1}.

The three relaxation times, $1/\tau_2$, $1/\tau_3$, and $1/\tau_4$, for the considered sequential four-step reaction show characteristic, hyperbolic dependence upon [ligand] reaching the plateau values at higher [ligand]. Thus, in the high ligand concentration range, the values of $1/\tau_2$, $1/\tau_3$, and $1/\tau_4$ become independent of the ligand concentration. It is also evident that, for the selected values of the rate constants, $1/\tau_3$ and $1/\tau_4$ reach their plateaus at a lower ligand concentration than $1/\tau_2$. On the other hand, the largest reciprocal of relaxation time, $1/\tau_1$, passes a nonlinear region at low protein concentrations and increases linearly with the protein concentration in the high concentration range (*24*, *25*). This is typical behavior for the relaxation time characterizing the bimolecular binding process (*37*). Notice that with the selected rate constants, the value of $1/\tau_1$ is already above 1000 s^{-1} and is strongly increasing even in the low ligand concentration range. Such a high value of $1/\tau_1$ makes its accurate determination very difficult in a standard stopped-flow experiment, with a typical dead-time of ~1−2 ms. The entire fast process, characterized by τ_1, is hidden in the unresolved fast change of the observed signal (e.g., fluorescence) from the time $t = 0$ to the steady-state value of the signal before the flow stops. However, if the amplitude of the fast process can be recovered from the data, and the simultaneous analysis of all amplitudes and relaxation times is performed, then the values of rate constants for the bimolecular step can be obtained with adequate accuracy (see below). This is because the amplitudes, like relaxation times, are very sensitive functions of spectroscopic parameters and rate constants of the reaction (*24*, *25*).

Amplitudes. The effect of the rate constants characterizing the bimolecular step on the dependence of individual amplitudes, A_1, A_2, A_3, and A_4, of the reaction upon the ligand concentration is shown in Figure 2 a−d. The amplitudes are normalized i.e., they are expressed as fractions ($A_i/\Sigma A_i$) of the total amplitude, $A_{tot} = \Sigma A_i$. The computer simulations were performed, using eqs 19a−d, for different sets of rate constants for the bimolecular step but the same set of spectroscopic parameters characterizing each intermediate. Also, although the values of the rate constants are changed, the equilibrium constant for the first step, $K_1 = k_1/k_{-1}$, is held constant, thus preserving the same free energy change accompanying the first step of the reaction. The selected molar fluorescence intensities of intermediates, with respect to the fluorescence intensity of the free ligand $F_1 = 1$, are $F_2 = 1.3$, $F_3 = 2$, $F_4 = 2$, and $F_5 = 2$.

The plots show several very characteristic features of the behavior of the examined system. At low ligand concentrations, mainly the amplitude A_4, of the fourth normal mode of the reaction, contributes to the observed kinetic trace at any value of the rate constants k_1 and k_{-1}. Such behavior is not a result of a dominant fluorescence intensity of N_5, as often suggested, but a low efficiency of the formation of N_2, N_3, and N_4 (*24*, *25*). The amplitude of the third normal mode, A_3, is always bell-shaped; however, the value of its maximum decreases with increased values of k_1 and k_{-1}. Notice that if the experiments are performed at higher ligand concentrations, only one side of the bell-shaped curve of A_3

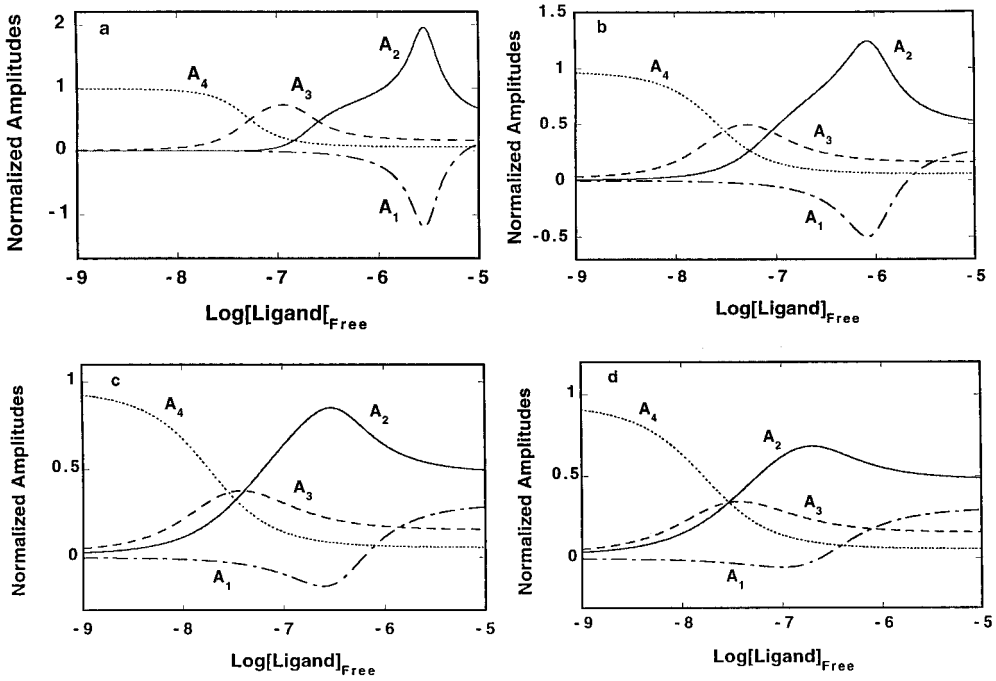

FIGURE 2: Computer simulation of the dependence of individual, A_1, A_2, A_3, and A_4, relaxation amplitudes for the four-step sequential mechanism of ligand binding to a macromolecule, defined by eq 2, upon the logarithm of the free ligand concentration, for the same set of relative molar fluorescence intensities, but with different values of rate constants, k_1 and k_{-1}, characterizing the bimolecular binding step. The relative fluorescence intensities, F_2, F_3, F_4, and F_5, corresponding to intermediates, N_2, N_3, N_4, and N_5, are 1.3, 2, 2, and 2, respectively. The fluorescence of the free macromolecule, N_1, is taken as $F_1 = 1$. The individual amplitudes are expressed as fractions of the total amplitude A_{tot}. The simulations have been performed with the same set of remaining rate constants: $k_2 = 600\ s^{-1}$, $k_{-2} = 250\ s^{-1}$, $k_3 = 50\ s^{-1}$, $k_{-3} = 10\ s^{-1}$, $k_4 = 10\ s^{-1}$, and $k_{-4} = 3\ s^{-1}$. (a) $k_1 = 3 \times 10^8\ M^{-1}\ s^{-1}$, $k_{-1} = 30\ s^{-1}$. (b) $k_1 = 1 \times 10^9\ M^{-1}\ s^{-1}$, $k_{-1} = 100\ s^{-1}$. (c) $k_1 = 3 \times 10^9\ M^{-1}\ s^{-1}$, $k_{-1} = 300\ s^{-1}$. (d) $k_1 = 6 \times 10^9\ M^{-1}\ s^{-1}$, $k_{-1} = 600\ s^{-1}$. A_1 (− - −), A_2 (—), A_3 (− −), A_4 (•••).

will be recorded and the amplitude will appear as continuously decaying with the increasing ligand concentration. Amplitude A_2 shows behavior similar to that of A_3, but the values of k_1 and k_{-1} affect not only the value and the location of the A_2 maximum but also the amplitude shape. The amplitude of the first normal mode, A_1, has very low values at lower ligand concentrations, independently of the values of k_1 and k_{-1}. However, the A_1 contribution increases with increased values of k_1 and k_{-1}. Moreover, at higher [ligand], A_1 begins to contribute substantially to the relaxation process. With the selected F_2 lower than other molar fluorescence intensities, A_1 assumes both negative and positive values and exhibits the maximum depending on the values of k_1 and k_{-1}. Also, the shape and the location of the A_1 minimum depend on k_1 and k_{-1}. Notice that, although the value of equilibrium constant K_1 is unchanged, all amplitudes are shifted toward high ligand concentrations at lower values of k_1 and k_{-1}.

The effect of the spectroscopic parameter, F_2, characterizing the first intermediate, N_2, on the behavior of all amplitudes, is shown in Figure 3a−c. Independently, whether or not F_2 is a major fluorescence intensity, the amplitude of A_4 always dominates the relaxation process at low [ligand]. The seemingly small change of F_2 substantially affects the remaining amplitudes including the shape of both A_2 and A_3. Moreover, in the case where F_2 is the major fluorescence intensity (Figure 3c), A_3 and A_2 become negative in the high ligand concentration range. As expected, F_2 has the most dramatic effect on A_1. When F_2 is lower than the molar fluorescence intensities of the remaining intermediates, A_1 is negative over a large range of the ligand concentration and shows a well-pronounced minimum (Figure 3a). When the value of F_2 is the same or larger than F_3, F_4, and F_5, the amplitude A_1 is always positive, and has a typical sigmoidal shape. It becomes a dominant relaxation effect only at higher [ligand].

Computer simulations included in Figures 2 and 3 show that the analysis of the individual amplitudes of the reaction will allow the extraction the kinetic and spectroscopic properties of each step and intermediate of the reaction. This includes the fast bimolecular step, even if the relaxation time for this step is not directly resolved in the experiment.

RESULTS

Kinetics of Human Pol β Binding to the ssDNA 20-mer, dT(pT)$_8$-Flu-(pT)$_{10}$, in the (Pol β)$_{16}$ Binding Mode. Human pol β forms the high-affinity (pol β)$_{16}$ binding mode in excess of the ssDNA and low protein concentration (*19*−*23*). The transition to the low site-size (pol β)$_5$ binding mode occurs only at high enzyme concentrations, as a result of the increased binding density (degree of binding) of the protein on the nucleic acid lattice or as a result of the limited access to the DNA, as in the case of the short ssDNA oligomers (*19, 20*). The difference between the affinities of the (pol β)$_{16}$ and (pol β)$_5$ binding modes and the resulting separation of both modes on the protein concentration scale allow us to study the kinetics of the (pol β)$_{16}$ binding mode formation, independently of the formation of the (pol β)$_5$ binding mode (*19, 20*).

The dynamics of the formation of the (pol β)$_{16}$ binding mode by human pol β have been addressed in the experiments with the ssDNA 20-mer. This oligomer is long enough to interact with the total DNA-binding site of the polymerase,

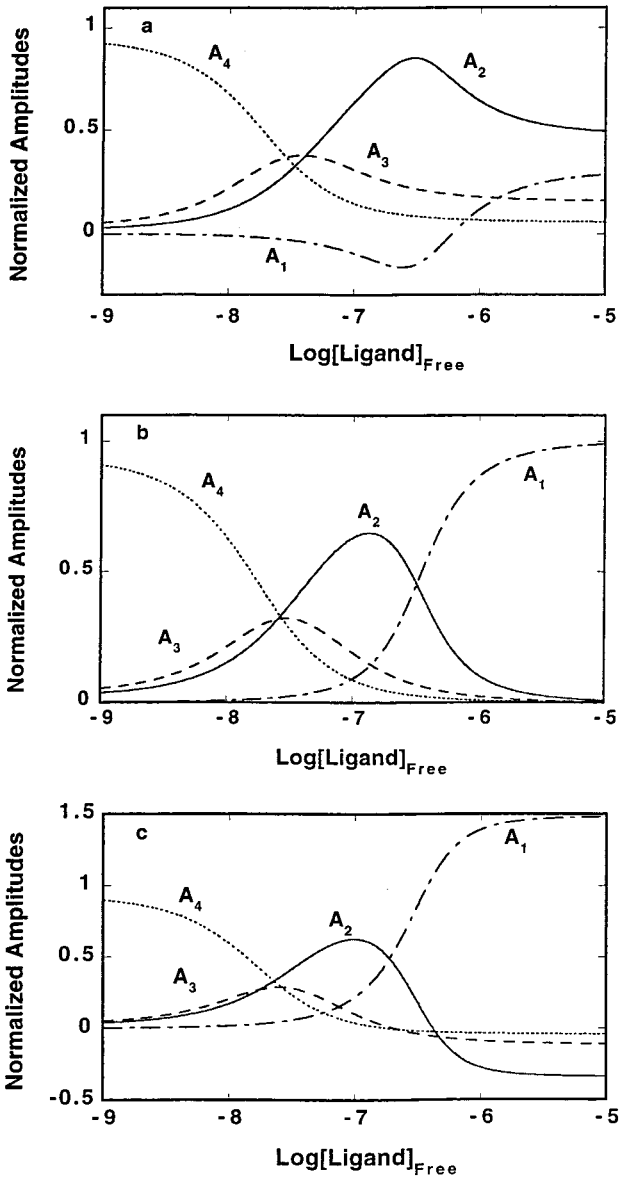

FIGURE 3: Computer simulation of the dependence of individual, A_1, A_2, A_3, and A_4, relaxation amplitudes for the four-step sequential mechanism of a ligand binding to a macromolecule, defined by eq 2, upon the logarithm of the free ligand concentration, for the same set of rate constants, but different relative molar fluorescence intensity, F_2, corresponding to the intermediate, N_2. The fluorescence of the free macromolecule, N_1, is taken as $F_1 = 1$. The individual amplitudes are expressed as fractions of the total amplitude A_{tot}. The simulations have been performed with the constant set of rate constants: $k_1 = 3 \times 10^9$ M^{-1} s^{-1}, $k_{-1} = 300$ s^{-1}, $k_2 = 600$ s^{-1}, $k_{-2} = 250$ s^{-1}, $k_3 = 50$ s^{-1}, $k_{-3} = 10$ s^{-1}, $k_4 = 10$ s^{-1}, and $k_{-4} = 3$ s^{-1}, and with the constant set of values $F_3 = 2$, $F_4 = 2$, and $F_5 = 2$. (a) $F_2 = 1.3$. (b) $F_2 = 2$. (c) $F_2 = 2.5$. A_1 (− - −), A_2 (—), A_3 (− −), A_4 (•••).

which occludes 16 ± 2 nucleotide residues (*19, 20*). In our previous thermodynamic studies of human pol β interactions with ssDNA, we used the fluorescent etheno derivative of the nucleic acid to examine the binding process (*19, 20*). However, we found that the observed signal is not adequate enough to quantitatively examine the very complex kinetics of the reaction (data not shown). On the other hand, we have found that binding of the enzyme to the ssDNA 20-mer containing the fluorescein residue, e.g., dT(pT)$_8$-pFlu-(pT)$_{10}$, is accompanied by a significant fluorescence increase of the

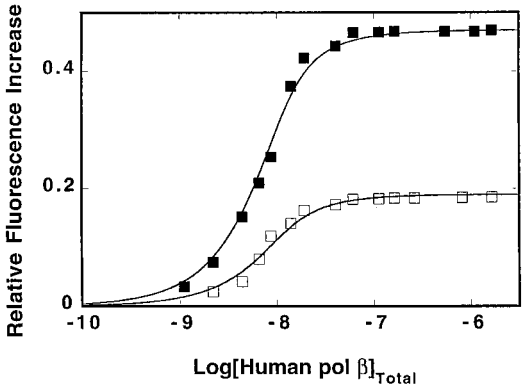

FIGURE 4: Fluorescence titrations of dT(pT)$_8$-pFlu-(pT)$_{10}$ (λ_{ex} = 485 nm, λ_{em} = 520 nm) with human pol β in buffer C (pH 7.0, 10 °C), containing 50 mM NaCl (■) or containing 50 mM NaCl and 1 mM $MgCl_2$ (□). The solid lines are computer fits of the binding isotherms to a single-site binding isotherm: $\Delta F = \Delta F_{max}(K_{20}[\text{enzyme}]_{free}/(1 + K_{20}[\text{enzyme}]_{free}))$. The concentration of dT(pT)$_8$-pFlu-(pT)$_{10}$ is 1×10^{-8} M (oligomer) (details in text).

DNA, providing an excellent signal to monitor the kinetics of polymerase−ssDNA complex formation. The fluorescein residue has a high quantum yield that allows us to perform experiments at a very low nucleic acid concentration. Any contribution of the protein fluorescence to the observed traces is eliminated by the excitation at 485 nm. Moreover, the mechanism of binding is independent of the location of the fluorescein in the ssDNA oligomer (see below).

Fluorescence titrations of dT(pT)$_8$-pFlu-(pT)$_{10}$ with human pol β in buffer C (pH 7.0, 10 °C), containing 50 mM NaCl, are included in Figure 4. The titrations have been performed in the limited protein concentration range ($<1.5 \times 10^{-6}$ M) to avoid the formation of the (pol β)$_5$ binding mode. As we discussed above, this is possible because of the large difference in affinities between the two ssDNA-binding modes (*19, 20*). Thus, only the formation of the (pol β)$_{16}$ binding mode is observed. The solid line in Figure 4 is a computer fit of the experimental isotherm to a single-site binding isotherm, $\Delta F = \Delta F_{max}(K_{20}[\text{enzyme}]_{free}/(1 + K_{20}[\text{enzyme}]_{free}))$, where ΔF_{max} and K_{20} are the maximum fractional fluorescence increases at saturation (Materials and Methods) and the macroscopic binding constant of the human pol β to the 20-mer in the (pol β)$_{16}$ binding mode, respectively. Thus, the formation of the (pol β)$_{16}$ binding mode on dT(pT)$_8$-pFlu-(pT)$_{10}$ is characterized by $\Delta F_{max} = 0.47 \pm 0.05$ and $K_{20} = (5 \pm 1.2) \times 10^8$ M^{-1}, respectively.

The kinetic experiments have been performed under pseudo-first-order conditions by mixing the 20-mer with an excess of human pol β. The stopped-flow kinetic trace of the dT(pT)$_8$-pFlu-(pT)$_{10}$ fluorescence, after mixing 1×10^{-7} M oligomer with 8×10^{-7} M human pol β (final concentrations) in buffer C (pH 7.0, 10 °C), containing 50 mM NaCl, is shown in Figure 5a. To increase the resolution, the plot is shown in logarithmic scale with respect to the time. There is an initial ~2 ms horizontal part of the trace (not considered in the fitting procedures) that corresponds to the steady-state fluorescence intensity recorded for 2 ms in our instrument before the flow stops (Materials and Methods). The observed kinetics are complex, and even a visual inspection shows the presence of multiple steps. A slower relaxation process follows a fast, initial process, both characterized by positive amplitudes. However, there is also a third process that is

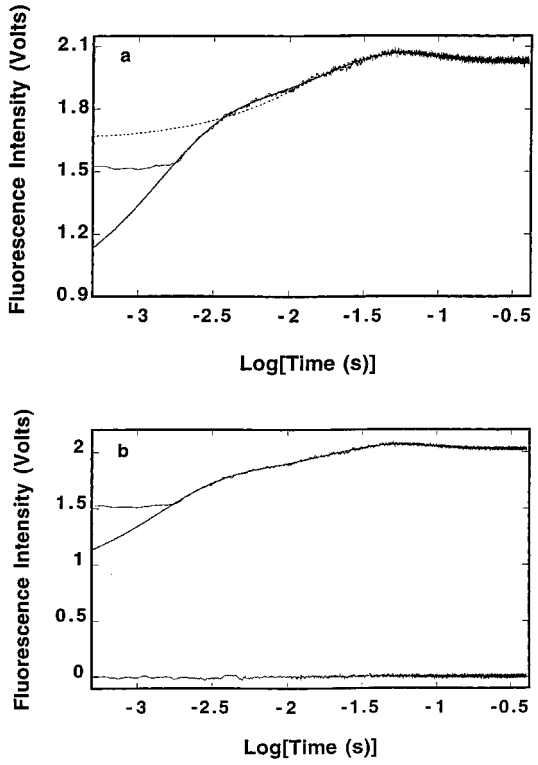

FIGURE 5: (a) Fluorescence stopped-flow kinetic trace, after mixing human pol β with the 20-mer, dT(pT)$_8$-pFlu-(pT)$_{10}$, in buffer C (pH 7.0, 10 °C), containing 50 mM NaCl (λ_{ex} = 485 nm, λ_{em} > 495 nm). The final concentrations of the polymerase and the 20-mer are 8×10^{-7} M and 1×10^{-7} M (oligomer), respectively. To increase the resolution, the experimental kinetic trace is shown in logarithmic scale with respect to time. The horizontal part of the trace is the steady-state value of the fluorescence of the sample recorded 2 ms before the flow stopped (Materials and Methods). The solid line is the three-exponential, nonlinear least-squares fit of the experimental curve using eq 1. The dashed line is the nonlinear least-squares fit using the two-exponential function (eq 1). (b) The same fluorescence stopped-flow trace as in panel a together with the zero line trace (lower trace) which is obtained after mixing the nucleic acid only with the buffer. The solid line is the same three-exponential, nonlinear least-squares fit of the experimental curve as shown in Figure 3a.

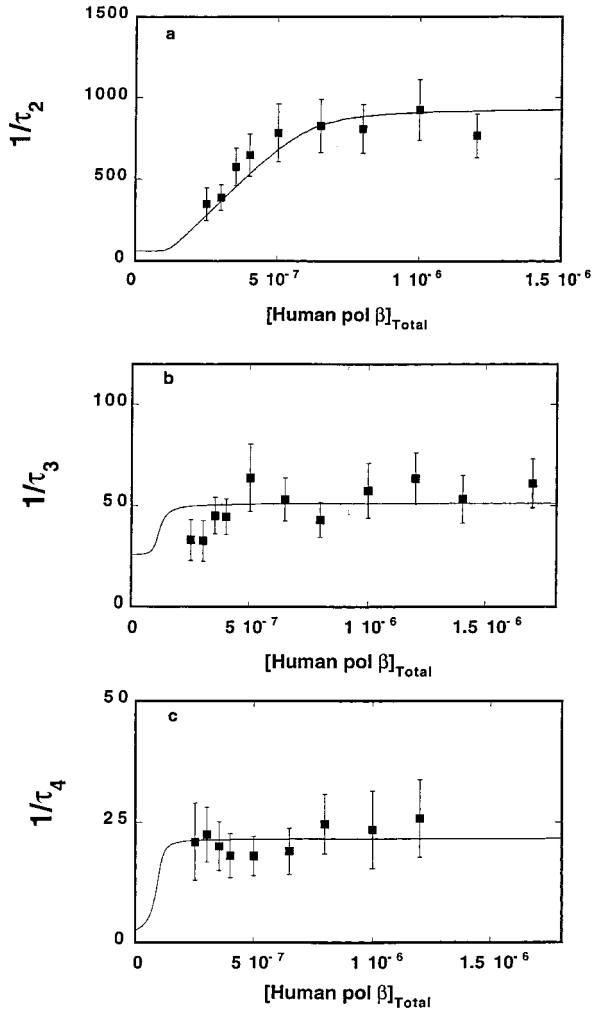

FIGURE 6: Dependence of the reciprocal relaxation times (s^{-1}) for the binding of human pol β to the 20-mer, dT(pT)$_8$-pFlu-(pT)$_{10}$, in the (pol β)$_{16}$ binding mode, in buffer C (pH 7.0, 10 °C), containing 50 mM NaCl, upon the total concentration of the enzyme. The solid lines are nonlinear least-squares fits according to the four-step sequential mechanism, defined by Scheme 1, with the rate constants: $k_1 = 1.8 \times 10^9$ M^{-1} s^{-1}, $k_{-1} = 40$ s^{-1}, $k_2 = 570$ s^{-1}, $k_{-2} = 350$ s^{-1}, $k_3 = 50$ s^{-1}, $k_{-3} = 15$ s^{-1}, $k_4 = 10$ s^{-1}, and $k_{-4} = 18$ s^{-1} (details in text). (a) $1/\tau_2$. (b) $1/\tau_3$. (c) $1/\tau_4$. The error bars are standard deviations obtained from 3−4 independent experiments.

characterized by a negative fluorescence change. The solid line in Figure 5a is a nonlinear least-squares fit of the experimental curve using a three-exponential fit which provides an excellent description of the kinetic trace. It is evident that the two-exponential fit (dashed line) is not sufficient to describe the observed kinetics.

The same kinetic trace depicted in Figure 5a, together with the trace corresponding to the nucleic acid alone (zero line), at the same concentration as used with the protein but mixed only with the buffer, is shown in Figure 5b. These data show that although the three-exponential fit provides an excellent description of the recorded trace, it does not account for the observed, total fluorescence increase which results from the complex formation. The difference between the fluorescence intensity of the end point of the kinetic trace and the zero line recorded for the nucleic acid alone is the total amplitude of the reaction, A_{tot} (eq 15). Thus, the data indicate that there is at least one additional fast step preceding the observed trace, characterized by the relaxation time τ_1, that is too short to be determined in the stopped-flow experiment. Therefore, the association of human pol β with the ssDNA 20-mer in the (pol β)$_{16}$ binding mode is a process that includes at least four steps.

The reciprocal relaxation times, $1/\tau_2$, $1/\tau_3$, and $1/\tau_4$, extracted from the experimental trace, as a function of the total human pol β concentration, are shown in Figure 6a−c. The value of $1/\tau_2$ shows hyperbolic dependence upon [human pol β], while both $1/\tau_3$ and $1/\tau_4$ are, within experimental accuracy, independent of enzyme concentration. Such behavior indicates that all three relaxation times characterize the intramolecular transitions of the complex (Figure 1) (*24*, *25*, *37*). Therefore, the minimum mechanism which can account for the observed dependence of the relaxation times upon the human pol β concentration and the presence of the third unresolved process is a four-step, sequential binding reaction in which bimolecular association is followed by three isomerization steps, as described by Scheme 1.

Although one cannot determine the relaxation time, τ_1, for the fast normal mode, the amplitude of this mode, A_1,

Scheme 1

$$\text{Human pol } \beta + N \underset{k_{-1}}{\overset{k_1}{\Leftrightarrow}} (P_{16}-\text{ssDNA})_1 \underset{k_{-2}}{\overset{k_2}{\Leftrightarrow}} (P_{16}-\text{ssDNA})_2 \underset{k_{-3}}{\overset{k_3}{\Leftrightarrow}} (P_{16}-\text{ssDNA})_3 \underset{k_{-4}}{\overset{k_4}{\Leftrightarrow}} (P_{16}-\text{ssDNA})_4$$

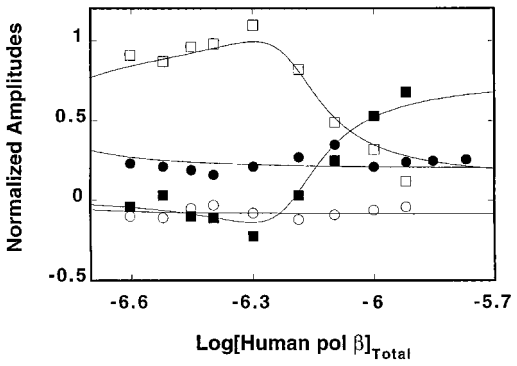

FIGURE 7: Dependence of the individual relaxation amplitudes, A_1, A_2, A_3, and A_4, for the binding of human pol β to the 20-mer, dT-$(pT)_8$-pFlu-$(pT)_{10}$, in buffer C (pH 7.0, 10 °C), containing 50 mM NaCl, upon the logarithm of the total enzyme concentration. The solid lines are nonlinear least-squares fits according to the four-step sequential mechanism, defined by Scheme 1, with the relative fluorescence intensities $F_2 = 1.344$, $F_3 = 1.456$, $F_4 = 1.531$, and $F_5 = 1.375$. The maximum nucleic acid fluorescence increase is taken from the equilibrium fluorescence titration in the same solution conditions as $\Delta F_{max} = 0.47$ (details in text). The rate constants are the same as in Figure 6. A_1 (■), A_2 (□), A_3 (●), A_4 (○).

can be obtained from the known amplitudes of the second, third, and fourth normal modes, A_2, A_3, and A_4, and the total amplitude of the reaction, A_{tot}, from eq 18, as

$$A_1 = A_{tot} - A_2 - A_3 - A_4 \qquad (19)$$

The dependence of the individual amplitudes, A_1, A_2, A_3, and A_4, of the four relaxation steps upon the human pol β concentration is shown in Figure 7. The individual amplitudes are expressed as fractions of the total amplitude, $A_i/\Sigma A_i$. In the examined enzyme concentration ranges, all four amplitudes contribute to the A_{tot}, even at the lowest [enzyme]. The positive amplitude, A_2, goes through a maximum, while the positive A_3 steadily decreases with the [human pol β]. Amplitude A_4 has a negative value over the entire [polymerase] range. On the other hand, A_1 initially has a negative value and shows a minimum at intermediate enzyme concentrations. As the concentration of the polymerase increases, A_1 assumes positive values and becomes a dominant relaxation effect. Such behavior of the individual amplitudes is in full agreement with the proposed mechanism (Scheme 1; Figures 2 and 3).

Because only three relaxation times are available from the experiment, the determination of rate constants of particular steps and molar fluorescence parameters characterizing each intermediate requires the simultaneous analyses of both the relaxation times and the amplitudes. We applied the following strategy to obtain all rate and spectroscopic parameters of the system (*24, 25*). We utilized the fact that we know the value of the macroscopic binding constant $K_{20} = (5 \pm 1.2) \times 10^8\ M^{-1}$ independently obtained in the same solution conditions by the equilibrium fluorescence titration method (Figure 4). The macroscopic binding constant K_{20} is related to the equilibrium constants characterizing partial equilibrium steps by

$$K_{20} = K_1(1 + K_2 + K_2K_3 + K_2K_3K_4) \qquad (20)$$

where $K_1 = k_1/k_{-1}$, $K_2 = k_2/k_{-2}$, $K_3 = k_3/k_{-3}$, and $K_4 = k_4/k_{-4}$. This relationship reduces the number of independent parameters to 5 in the numerical fitting of the three individual relaxation times. Because the unresolved step is very fast, the fit is first performed with the starting value of the rate constant k_1 close to the diffusion-controlled limit, e.g., $\sim 5 \times 10^9\ M^{-1}$. Subsequently, various values of k_1 and other rate constants have been tested in these analyses.

The obtained rate constants were then used in the fitting of the four individual amplitudes that include the relative molar fluorescence intensities. This can be accomplished by using the matrix projection operator technique, which allows us to determine the molar fluorescence intensities characterizing each intermediate of the reaction, i.e., to assess the conformational state of the protein−nucleic acid complex in each intermediate. The determination is also facilitated by the fact that the maximum, fractional increase of the nucleic acid fluorescence, $\Delta F_{max} = 0.47 \pm 0.05$, is known from the equilibrium titrations (Figure 4). Moreover, ΔF_{max} can be analytically expressed as (*19, 20*)

$$\Delta F_{max} = \frac{\Delta F_2}{Z} + \frac{K_2\Delta F_3}{Z} + \frac{K_2K_3\Delta F_4}{Z} + \frac{K_2K_3K_4\Delta F_5}{Z} \qquad (21)$$

where $Z = 1 + K_2 + K_2K_3 + K_2K_3K_4$, $\Delta F_2 = (F_2 - F_1)/F_1$, $\Delta F_3 = (F_3 - F_1)/F_1$, $\Delta F_4 = (F_4 - F_1)/F_1$, and $\Delta F_5 = (F_5 - F_1)/F_1$ are the fractional fluorescence intensities of each intermediate in the binding of human pol β to the ssDNA 20-mer in the $(\text{pol } \beta)_{16}$ binding mode, relative to the molar fluorescence intensity of the free nucleic acid, F_1. It should be pointed out that contrary to ΔF_i, the fluorescence parameters, F_2, F_3, F_4, and F_5, are relative molar fluorescence intensities, not fractional intensities, with respect to the free nucleic acid fluorescence. Equation 21 provides an additional relationship between the fluorescence parameters. The value of ΔF_{max} simply plays the role of a scaling factor. In the final step of the analysis, global fitting that simultaneously includes all relaxation times and amplitudes refined the values of the rate constants and relative molar fluorescence parameters.

The solid lines in Figures 6 and 7 are computer fits of the relaxation times and amplitudes according to the above mechanism, using a single set of the parameters. The obtained rate constants and relative molar fluorescence parameters for the mechanism defined by Scheme 1 are included in Table 1.

Introducing the values of the rate constants into the partial equilibrium constants for each step provides $K_1 = (4.6 \pm 1.6) \times 10^7\ M^{-1}$, $K_2 = 1.6 \pm 0.5$, $K_3 = 3.3 \pm 0.7$, and $K_4 = 0.6 \pm 0.3$ (Table 1). Thus, the first step has a dominant contribution to the free energy, $\Delta G°$, of ssDNA binding. The next two steps also increase the affinity, while the fourth

Table 1: Kinetic, Thermodynamic, and Spectroscopic Parameters Characterizing the Binding of Human Pol β to dT(pT)$_8$-pFlu-(pT)$_{10}$, dT(pT)$_{14}$-pFlu-(pT)$_4$, and dA(pA)$_8$-pFlu-(pA)$_{10}$ in the (Pol β)$_{16}$ Binding Mode, and dT(pT)$_3$-pFlu-(pT)$_5$ in the (Pol β)$_5$ Binding Mode, in Buffer C (pH 7, 10 °C), Containing 50 mM NaCl

oligomer	$k_{1\|}$ (M^{-1} s^{-1})	k_{-1} (s^{-1})	k_2 (s^{-1})	k_{-2} (s^{-1})	k_3 (s^{-1})	k_{-3} (s^{-1})	k_4 (s^{-1})	k_{-4} (s^{-1})	K_1 (M^{-1})	K_2	K_3	K_4	K_M[a] (M^{-1})	F_2[b]	F_3[b]	F_4[b]	F_5[b]
dT(pT)$_8$pFlu-(pT)$_{10}$	$(1.8 \pm 0.3) \times 10^9$	40 ± 10	570 ± 80	350 ± 30	50 ± 8	15 ± 4	10 ± 3	18 ± 4	$(4.6 \pm 1.6) \times 10^7$	1.6 ± 0.5	3.3 ± 0.7	0.6 ± 0.3	$(5 \pm 1.2) \times 10^8$	1.35 ± 0.05	1.46 ± 0.05	1.53 ± 0.05	1.38 ± 0.05
dT(pT)$_{14}$pFlu-(pT)$_4$	$(1.5 \pm 0.3) \times 10^9$	55 ± 9	370 ± 60	270 ± 25	55 ± 9	18 ± 5	7 ± 2	15 ± 3	$(2.7 \pm 0.9) \times 10^7$	1.4 ± 0.5	3.1 ± 0.6	0.47 ± 0.25	$(5.5 \pm 1.2) \times 10^8$	1.33 ± 0.05	1.41 ± 0.05	1.45 ± 0.05	1.46 ± 0.05
dT(pT)$_3$pFlu-(pT)$_5$	$(2 \pm 0.4) \times 10^9$	300 ± 60	90 ± 20	400 ± 60	30 ± 10	48 ± 10	5 ± 1.5	19 ± 4	$(6.7 \pm 2) \times 10^6$	0.23 ± 0.09	0.63 ± 0.3	0.26 ± 0.1	$(9.4 \pm 1.5) \times 10^6$	1.03 ± 0.02	1.17 ± 0.05	1.48 ± 0.05	1.22 ± 0.05
dA(pA)$_8$pFlu-(pA)$_{10}$	$(1.8 \pm 0.3) \times 10^9$	100 ± 40	270 ± 60	170 ± 40	37 ± 5	32 ± 3	−	−	$(1.8 \pm 0.8) \times 10^7$	1.6 ± 0.6	1.16 ± 0.2	−	$(8 \pm 2) \times 10^7$	1.2 ± 0.05	1.34 ± 0.05	1.37 ± 0.05	−

[a] K_M (equilibrium macroscopic binding constant) is referred to in the text as K_{20} for the 20-mers and K_{10} for the 10-mer, respectively. [b] Values relative to the fluorescence, $F_1 = 1$, of the free ssDNA oligomers (details in text).

step has a negative contribution to $\Delta G°$. The data indicate that the first intermediate, (P-ssDNA)$_1$, is characterized by the largest relative molar fluorescence intensity ($F_2 = 1.35 \pm 0.05$), as compared to the free 20-mer. The conformational transition to (P$_{16}$-ssDNA)$_2$ induces only an ~7% additional increase of the 20-mer fluorescence over F_2 ($F_3 = 1.46 \pm 0.05$), the transition to the (P$_{16}$-ssDNA)$_3$ is accompanied by an additional increase of the ssDNA fluorescence by ~7% as compared to F_3 ($F_4 = 1.53 \pm 0.05$), but transition to the (P$_{16}$-ssDNA)$_4$ is accompanied by the nucleic acid fluorescence decrease as compared to F_4 ($F_5 = 1.38 \pm 0.05$) (see Discussion).

Kinetics of (Pol β)$_5$ Binding Mode Formation. Stopped-Flow Studies of Human Pol β Binding to the ssDNA 10-mer, dT(pT)$_3$-pFlu-(pT)$_5$. Human pol β binds the ssDNA in the (pol β)$_5$ binding mode when the access or availability of the nucleic acid is diminished (*20*). In this binding mode, the polymerase associates with only 5 ± 2 nucleotide residues, exclusively engaging its 8-kDa domain in the interactions with the DNA (*19, 20*). This ability of the polymerase to adjust its site-size in the complex with the nucleic acid may play a key role in the recognition of the small ssDNA gaps of the damaged DNA (*19*−*23*). Thus, elucidation of the mechanism of formation of (pol β)$_5$ binding is crucial for our understanding of the recognition processes by the polymerase. To address this issue, we examined the kinetics of human pol β binding to the ssDNA 10-mer, dT(pT)$_3$-pFlu-(pT)$_5$. Our previous studies showed that with the ssDNA oligomer 10 nucleotide residues long, the enzyme can only form the (pol β)$_5$ binding mode (*19, 22, 23*).

The stopped-flow experiments have been performed under pseudo-first-order conditions by mixing the dT(pT)$_3$-pFlu-(pT)$_5$ with a large excess of human pol β. The stopped-flow kinetic trace of the dT(pT)$_3$-pFlu-(pT)$_5$ fluorescence, after mixing 1×10^{-7} M (oligomer) 10-mer with 8×10^{-7} M human pol β (final concentrations) in buffer C (pH 7.0, 10 °C), containing 50 mM NaCl, is shown in Figure 8. Also, the trace corresponding to the nucleic acid alone (zero line), at the same concentration as used with the protein, but mixed only with the buffer, is included. The solid line is the three-exponential fit of the trace (eq 1). The two-exponential fit (dashed line) does not provide an adequate description of the experimental trace as expressed in the value of the variance of the two-exponential fit which is ~35% higher. As observed in the case of formation of the (pol β)$_{16}$ binding mode, although the three-exponential fit provides an excellent description of the observed kinetics, it does not account for the entire fluorescence increase which results from the

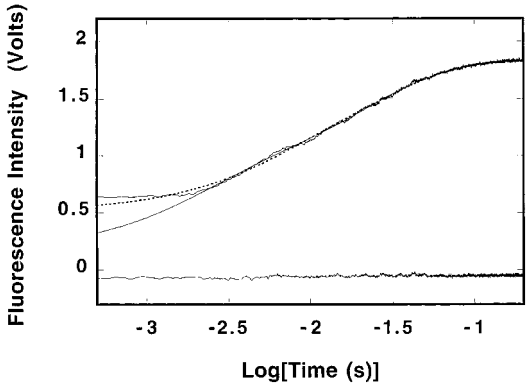

FIGURE 8: Fluorescence stopped-flow kinetic trace, after mixing human pol β with the 10-mer, dT(pT)$_3$-pFlu-(pT)$_5$, in buffer C (pH 7.0,10 °C), containing 50 mM NaCl ($\lambda_{ex} = 485$ nm, $\lambda_{em} > 495$ nm). The final concentrations of the polymerase and the 10-mer are 8×10^{-7} M and 1×10^{-7} M (oligomer), respectively. To increase the resolution, the experimental kinetic trace is shown in logarithmic scale with respect to time. The initial, horizontal part of the trace is the steady-state value of the fluorescence of the sample recorded for 2 ms before the flow stopped (Materials and Methods). The solid line is the three-exponential, nonlinear least-squares fit of the experimental curve using eq 1. The dashed line is the nonlinear least-squares fit using the two-exponential function. The lower horizontal trace is the zero line, which is obtained after only mixing the nucleic acid with the buffer.

complex formation. The data indicate that there is a fast step preceding the observed trace, characterized by a relaxation time too short to be extracted in the stopped-flow experiment. In other words, the formation of the (pol β)$_5$ binding mode also includes at least four steps.

The reciprocal relaxation times, $1/\tau_2$, $1/\tau_3$, and $1/\tau_4$, characterizing the three relaxation processes, as a function of the total human pol β concentration, are shown in Figure 9a−c. All three relaxation times show little dependence upon [enzyme], indicating that they characterize isomerizations of the formed complex (Figures 2 and 6) (*24, 25*). The simplest mechanism of the formation of the (pol β)$_5$ binding mode, which can account for such behavior of the relaxation times, is a sequential, four-step reaction in which the bimolecular association is followed by three conformational transitions of the formed complex, as described by Scheme 2, analogous to Scheme 1. This conclusion is fully supported by the amplitude analysis (described below).

Although, the relaxation time τ_1 is not available from the experiment, the amplitude A_1 of this mode can be obtained from the known amplitudes of the second, third, and fourth normal modes, A_2, A_3, and A_4, and the total amplitude of the reaction, as defined by eq 18. The dependence of the

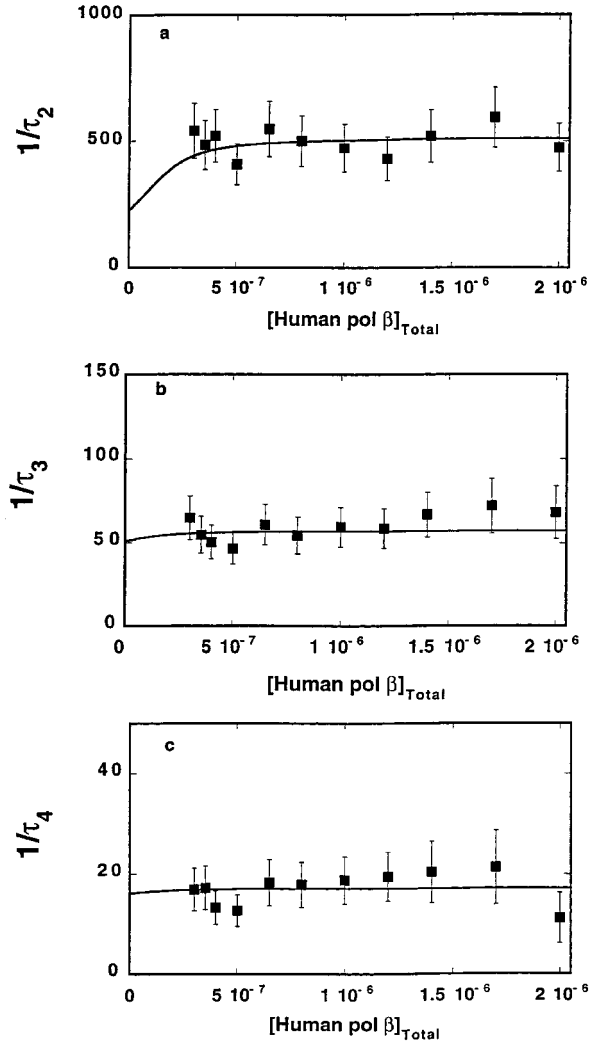

FIGURE 9: Dependence of the reciprocal relaxation times (s^{-1}) for the binding of human pol β to the 10-mer, $dT(pT)_3$-pFlu-$(pT)_5$, in buffer C (pH 7.0, 10 °C), containing 50 mM NaCl, upon the total concentration of the enzyme. The solid lines are nonlinear least-squares fits according to the four-step sequential mechanism, defined by Scheme 2, with the rate constants: $k_1 = 2 \times 10^9$ M^{-1} s^{-1}, $k_{-1} = 300$ s^{-1}, $k_2 = 90$ s^{-1}, $k_{-2} = 400$ s^{-1}, $k_3 = 30s^{-1}$, $k_{-3} = 48$ s^{-1}, $k_4 = 5$ s^{-1}, and $k_{-4} = 19$ s^{-1} (details in text). (a) $1/\tau_2$. (b) $1/\tau_3$. (c) $1/\tau_4$. The error bars are standard deviations obtained from 3−4 independent experiments.

individual amplitudes, A_1, A_2, A_3, and A_4, of the four relaxation steps upon the human pol β concentration is shown in Figure 10. The individual amplitudes are expressed as fractions of the total amplitude, $A_i/\Sigma A_i$. With the exception of A_1, all individual amplitudes significantly contribute to the total amplitude over the entire examined protein concentration range. While A_2, A_3, and A_4 are positive, A_1 assumes negative values at the low protein concentration and rises to positive values at the high [enzyme] range. Such behavior is in full agreement with the proposed mechanism (Scheme 2) and already indicates that the first intermediate has a relative molar fluorescence intensity significantly lower than the corresponding parameters characterizing other intermediates (Figures 2 and 3).

The same strategy, relying on the simultaneous analyses of the three relaxation times and the four amplitudes, as discussed above for (pol $\beta)_{16}$ binding mode formation, has been used to determine all rate constants of the particular steps and molar fluorescence parameters characterizing each intermediate in the (pol $\beta)_5$ binding mode formation (Figures 6 and 7). The macroscopic binding constant, $K_{10} = (9.4 \pm 1.5) \times 10^6$ M^{-1}, and the maximum, fractional increase of the nucleic acid fluorescence, $\Delta F_{max} = 0.22 \pm 0.02$, for the single human pol β molecule binding to $dT(pT)_3$-Flu-$(pT)_5$ have been independently obtained in the same solution conditions by the equilibrium fluorescence titration method (data not shown). Both quantities are analytically related to the partial equilibrium constants and fractional fluorescence changes of each intermediate by expressions analogous to eqs 20 and 21, respectively. The solid lines in Figures 9 and 10 are computer fits of the relaxation times and amplitudes according to the mechanism defined by Scheme 2, using a single set of parameters. The obtained rate constants and relative molar fluorescence parameters for the formation of the (pol $\beta)_5$ binding mode are included in Table 1.

The bimolecular step in the formation of the (pol $\beta)_5$ binding mode is similar to the analogous step determined for the (pol $\beta)_{16}$ binding mode; however, the dissociation rate constant k_{-1} is a factor of ~8 larger than the corresponding value obtained for the large site-size binding mode. On the other hand, transition to the second intermediate, $(P_5\text{-ssDNA})_2$, is characterized by a significantly lower (factor of ~6) rate constant than the analogous step in the formation of the (pol $\beta)_{16}$ binding mode (Table 1). Introducing the values of the rate constants to the equilibrium constants for each step provides $K_1 = (6.7 \pm 2) \times 10^6$ M^{-1}, $K_2 = 0.23 \pm 0.09$, $K_3 = 0.63 \pm 0.3$, and $K_4 = 0.26 \pm 0.1$. It is evident that, similar to the (pol $\beta)_{16}$ binding mode, the first step has a predominant contribution to the free energy of ssDNA binding, $\Delta G°$, in the formation of the (pol $\beta)_5$ binding mode. However, contrary to the results obtained with the ssDNA 20-mer, where only the last step contributes negatively to $\Delta G°$, all remaining steps in the formation of the (pol $\beta)_5$ binding mode contribute negatively to the free energy of binding (see Discussion).

There are also significant differences between the two ssDNA-binding modes in the structures of the intermediates, as indicated by their relative molar fluorescence intensities. The molar fluorescence intensity of the first intermediate in the (pol $\beta)_5$ binding mode is only ~3% larger than the fluorescence of the free nucleic acid, as compared to the ~35% difference in the case of the (pol $\beta)_{16}$ binding mode, indicating that a much less pronounced conformational nucleic acid change accompanies the formation of the first intermediate, $(P_5\text{-ssDNA})_1$, in the (pol $\beta)_5$ binding mode. Significant conformational changes occur in the transition to $(P_5\text{-ssDNA})_2$, and particularly to $(P_5\text{-ssDNA})_3$ which is characterized by the relative molar fluorescence intensity $F_4 = 1.48 \pm 0.05$, comparable to the (pol $\beta)_{16}$ binding mode intermediate $(P_{16}\text{-ssDNA})_3$ (Table 1) (see Discussion).

Stopped-Flow Kinetic Studies of Formation of the (Pol $\beta)_{16}$ and (Pol $\beta)_5$ Binding Modes in the Presence of Magnesium. Magnesium cations have a profound effect on human pol β interactions with ssDNA (*19, 21*). Our recent thermodynamic studies have shown that specific binding of Mg^{2+} to the 8-kDa domain of the analogous rat pol β not only affects the intrinsic interactions but also induces changes in the site-size of the protein−DNA complex (*19*−*21*).

Scheme 2

$$\text{Human pol } \beta + N \underset{k_{-1}}{\overset{k_1}{\Leftrightarrow}} (P_5-\text{ssDNA})_1 \underset{k_{-2}}{\overset{k_2}{\Leftrightarrow}} (P_5-\text{ssDNA})_2 \underset{k_{-3}}{\overset{k_3}{\Leftrightarrow}} (P_5-\text{ssDNA})_3 \underset{k_{-4}}{\overset{k_4}{\Leftrightarrow}} (P_5-\text{ssDNA})_4$$

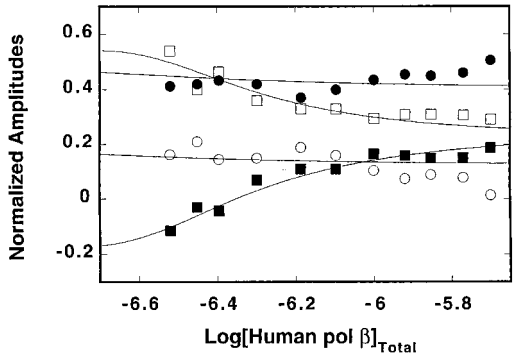

FIGURE 10: Dependence of the individual relaxation amplitudes, A_1, A_2, A_3, and A_4, for the binding of human pol β to the 10-mer, dT(pT)$_3$-pFlu-(pT)$_5$, in buffer C (pH 7.0, 10 °C), containing 50 mM NaCl, upon the logarithm of the total concentration of the enzyme. The solid lines are nonlinear least-squares fits according to the four-step sequential mechanism, defined by Scheme 2, with the relative molar fluorescence intensities $F_2 = 1.024$, $F_3 = 1.17$, $F_4 = 1.482$, and $F_5 = 1.22$. The maximum fluorescence increase of the nucleic acid is taken from the equilibrium fluorescence titration, in the same solution conditions as $\Delta F_{max} = 0.22$ (details in text). The rate constants are the same as in Figure 9. A_1 (■), A_2 (□), A_3 (●), A_4 (○).

Fluorescence titration of dT(pT)$_8$-pFlu-(pT)$_{10}$ with human pol β in buffer C (pH 7.0, 10 °C), containing 50 mM NaCl and 1 mM $MgCl_2$, is included in Figure 4. The solid line is a computer fit of the experimental isotherm to a single-site, binding isotherm (see above). The data show that the formation of the (pol β)$_{16}$ binding mode with dT(pT)$_8$-pFlu-(pT)$_{10}$, in the presence of $MgCl_2$, is characterized by $\Delta F_{max} = 0.19 \pm 0.02$ and $K_{20} = (3.5 \pm 1) \times 10^8$ M^{-1}, respectively. Notice that although the macroscopic binding constants are similar, the value of ΔF_{max} is significantly lower than that observed in the absence of magnesium, reflecting a different structure of the nucleic acid in the complex (Figure 4).

The effect of magnesium on the kinetics of (pol β)$_{16}$ binding mode formation was examined with dT(pT)$_8$-Flu-(pT)$_{10}$ in buffer C (pH 7.0, 10 °C), containing 50 mM NaCl and 1 mM $MgCl_2$ (data not shown). The obtained kinetic and spectroscopic parameters are included in Table 2. The presence of magnesium does not affect the reaction mechanism, but changes the internal energetics of the formed intermediates. The partial equilibrium constant K_1 is 30% lower in the presence of magnesium, indicating destabilization of the (P$_{16}$-ssDNA)$_1$ intermediate, while K_2 is unaffected. The value of K_3 is larger, thus, the presence of Mg^{2+} stabilizes the (P$_{16}$-ssDNA)$_3$. On the other hand, K_4 is a factor of ∼3 lower than in the absence of Mg^{2+} (Table 2). The intermediate (P$_{16}$-ssDNA)$_4$ is strongly destabilized in the presence of Mg^{2+}.

As already indicated by the equilibrium data, the presence of magnesium also affects the structural changes of the nucleic acid−enzyme complexes. The value of $F_2 = 1.01 \pm 0.03$ is virtually the same as the fluorescence intensity of the free nucleic acid, indicating that very little, if any, conformational changes occur in the formation of (P$_{16}$-ssDNA)$_1$. The major conformational changes take place in the formation of (P$_{16}$-ssDNA)$_2$ and (P$_{16}$-ssDNA)$_3$, although the relative molar intensities of these intermediates are lower than in the absence of Mg^{2+} (Tables 1 and 2). The relative molar fluorescence intensity of (P$_{16}$-ssDNA)$_4$ is even lower than the relative molar fluorescence intensity of the free nucleic acid (Table 2).

The effect of magnesium cations on the internal energetics of the formation of the (pol β)$_5$ binding mode is different (Table 2). The value of K_1 is decreased by a factor of ∼2, while the remaining partial equilibrium constants are not affected by the presence of Mg^{2+}. However, molar fluorescence intensities of all intermediates are lower in the presence of Mg^{2+}, indicating that significantly less pronounced conformational nucleic acid changes accompany their formation (Table 2). Nevertheless, contrary to the formation of the (pol β)$_{16}$ binding mode, the major conformational change of the nucleic acid in the formation of the (pol β)$_5$ binding mode in the presence of magnesium accompanies the transition to the intermediate (P$_5$-ssDNA)$_3$.

Stopped-Flow Kinetic Studies of (Pol β)$_{16}$ Binding Mode Formation with dA(pA)$_8$-pFlu-(pA)$_{10}$. In solution conditions applied in our studies, thymine oligomers form disordered structures with very limited base−base stacking interactions (*38*, *40*). On the other hand, adenosine homooligomers have an ordered conformation with significant stacking interactions between the bases (*39*, *40*). To address the role of the nucleic acid structure in the kinetics of (pol β)$_{16}$ binding mode formation by human pol β, we performed experiments with 20-mers, dA(pA)$_8$-pFlu-(pA)$_{10}$.

There is a significant difference between the kinetics of the (pol β)$_{16}$ binding mode formation with thymine versus the adenosine 20-mer. Stopped-flow kinetic traces for dA-(pA)$_8$-pFlu-(pA)$_{10}$ are adequately described not by the three- but by the two-exponential function (data not shown). However, as observed and discussed in the case of dT(pT)$_8$-pFlu-(pT)$_{10}$, the fit does not account for the amplitude of the fast initial step of the kinetic trace. Thus, the formation of the (pol β)$_{16}$ binding mode by human pol β with the dA-(pA)$_8$-pFlu-(pA)$_{10}$ includes at least three steps. The observed reciprocal relaxation times as well as the amplitudes characterizing the kinetics of polymerase binding to dA(pA)$_8$-pFlu-(pA)$_{10}$, as a function of the total enzyme concentration in buffer C (pH 7.0, 10 °C), containing 50 mM NaCl, are shown in Figure 11. Both $1/\tau_2$ and $1/\tau_3$ are independent of the polymerase concentration; i.e., they characterize intramolecular transitions. The amplitude A_1 increases with the increase of the [protein] and becomes the dominant relaxation effect at a higher enzyme concentration range. The amplitudes of the second (A_2) and third (A_3) normal modes decay as the [human pol β] increases. Such relaxation times and amplitude behavior indicate that the formation of the (pol β)$_{16}$ binding mode on dA(pA)$_8$-pFlu-(pA)$_{10}$ by human pol β is described by the three-step sequential mechanism where the bimolecular association is followed by two conformational transitions of the formed complex, as described by eq 22

Table 2: Kinetic, Thermodynamic, and Spectroscopic Parameters Characterizing the Binding of Human Pol β to dT(pT)$_8$-pFlu-(pT)$_{10}$ in the (Pol β)$_{16}$ Binding Mode, and dT(pT)$_3$-pFlu-(pT)$_5$ in the (Pol β)$_5$ Binding Mode, in Buffer C (pH 7, 10 °C), Containing 50 mM NaCl and 1 mM $MgCl_2$

oligomer	k_1 (M^{-1} s^{-1})	k_{-1} (s^{-1})	k_2 (s^{-1})	k_{-2} (s^{-1})	k_3 (s^{-1})	k_{-3} (s^{-1})	k_4 (s^{-1})	k_{-4} (s^{-1})	K_1 (M^{-1})	K_2	K_3	K_4	K_M[a] (M^{-1})	F_2[b]	F_3[b]	F_4[b]	F_5[b]
dT(pT)$_8$pFlu-(pT)$_{10}$	(2.7 ± 0.4) × 10^9	80 ± 25	480 ± 70	300 ± 40	60 ± 10	15 ± 3	5 ± 2	30 ± 6	(3.4 ± 1.4) × 10^7	1.6 ± 0.5	4 ± 1.5	0.17 ± 0.09	(3.5 ± 1) × 10^8	1.01 ± 0.03	1.19 ± 0.05	1.26 ± 0.05	0.96 ± 0.05
dT(pT)$_3$pFlu-(pT)$_5$	(1 ± 0.2) × 10^8	300 ± 50	100 ± 20	350 ± 60	30 ± 10	50 ± 16	5 ± 2	21 ± 4	(3.4 ± 1.2) × 10^6	0.29 ± 0.1	0.6 ± 0.3	0.24 ± 0.12	(5 ± 1.5) × 10^6	1.01 ± 0.02	1.05 ± 0.03	1.15 ± 0.05	1.07 ± 0.05

[a] K_M (equilibrium, macroscopic binding constant) is referred to in the text as K_{20} for the 20-mer and K_{10} for the 10-mer, respectively. [b] Values relative to the fluorescence, $F_1 = 1$, of the free ssDNA oligomers (details in text).

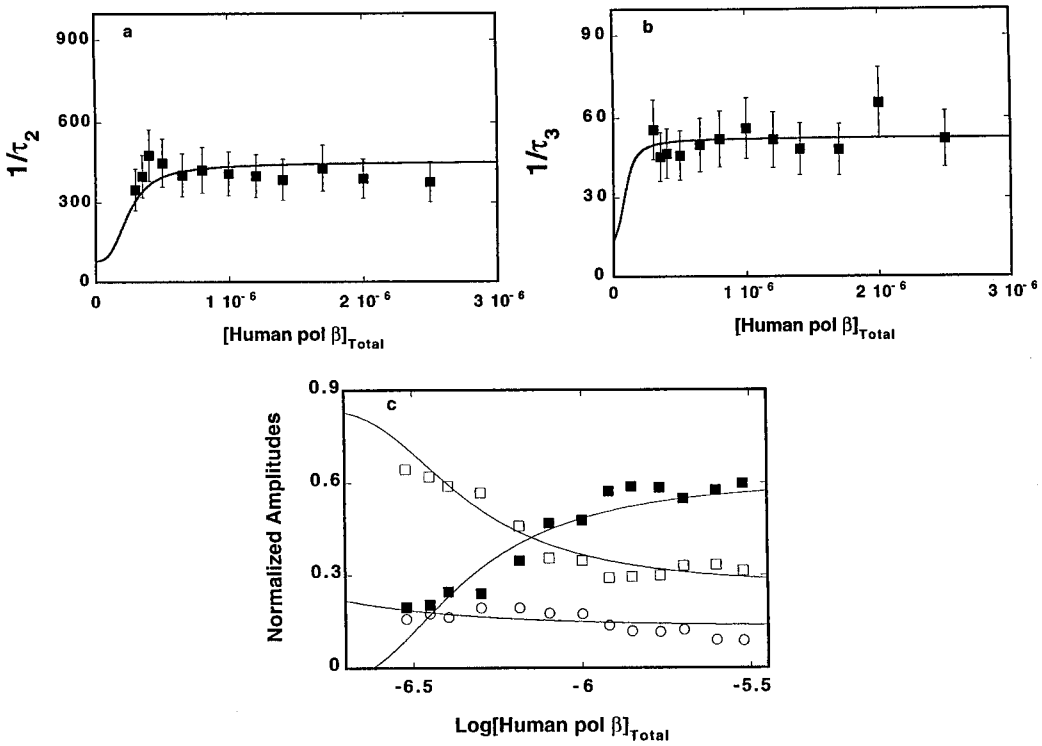

FIGURE 11: Dependence of the reciprocal relaxation times (s^{-1}) for the binding of human pol β to the 20-mer, dA(pA)$_8$-pFlu-(pA)$_{10}$, in buffer C (pH 7.0, 10 °C), containing 50 mM NaCl, upon the total concentration of the enzyme. The solid lines are nonlinear least-squares fits according to the three-step sequential mechanism, defined by eq 22, with rate constants: $k_1 = 1.8 \times 10^9$ M^{-1} s^{-1}, $k_{-1} = 100$ s^{-1}, $k_2 = 270 s^{-1}$, $k_{-2} = 170$ s^{-1}, $k_3 = 37$ s^{-1}, and $k_{-3} = 32$ s^{-1}. (a) $1/\tau_2$. (b) $1/\tau_3$. The error bars are standard deviations obtained from 3−4 independent experiments. (c) Dependence of the individual relaxation amplitudes, A_1, A_2, and A_3, for the binding of human pol β to the 20-mer, dA(pA)$_8$-pFlu-(pA)$_{10}$, in buffer C (pH 7.0, 10 °C), containing 50 mM NaCl, upon the total concentration of the enzyme. The solid lines are nonlinear least-squares fits according to the three-step sequential mechanism, defined by eq 22, with the relative molar fluorescence intensities $F_2 = 1.193$, $F_3 = 1.34$, and $F_4 = 1.37$. The maximum fluorescence increase of the nucleic acid is taken from the equilibrium fluorescence titration, in the same solution conditions as $\Delta F_{max} = 0.33$. The rate constants are the same as in Figure 9. A_1 (■), A_2 (□), A_3 (○).

$$\text{Human pol } \beta + \text{ssDNA} \underset{k_{-1}}{\overset{k_1}{\rightleftharpoons}} (P_{16}\text{-ssDNA})_1 \underset{k_{-2}}{\overset{k_2}{\rightleftharpoons}} (P_{16}\text{-ssDNA})_2 \underset{k_{-3}}{\overset{k_3}{\rightleftharpoons}} (P_{16}\text{-ssDNA})_3 \quad (22)$$

The analysis of the kinetic data was performed as described above for dT(pT)$_8$-pFlu-(pT)$_{10}$, using the macroscopic binding constant, $K_{20} = (8 \pm 2) \times 10^7$ M^{-1}, and the maximum fractional fluorescence increase, $\Delta F_{max} = 0.33 \pm 0.05$, determined in independent fluorescence titration experiments (data not shown). The obtained parameters are included in Table 1. The partial equilibrium constants are $K_1 = (1.8 \pm 0.8) \times 10^7$ M^{-1}, $K_2 = 1.6 \pm 0.6$, and $K_3 = 1.16 \pm 0.2$. The data indicate that similar to the thymine oligomer, in the formation of the (pol β)$_{16}$ binding mode on dA(pA)$_8$-pFlu-(pA)$_{10}$ all steps contribute favorably to the total free energy of binding $\Delta G°$. Nevertheless, the stability of the (P$_{16}$-ssDNA)$_3$ intermediate ($K_3 = 1.16 \pm 0.2$) is significantly lower than that observed in the case of dT(pT)$_8$-pFlu-(pT)$_{10}$ ($K_3 = 3.3 \pm 0.7$). However, the structural changes of the nucleic acid in different intermediates are less pronounced, as expressed by the lower values of the relative molar fluorescence intensities. Moreover, the conformational change of ssDNA in the formation of (P$_{16}$-ssDNA)$_1$ is not a dominant structural nucleic acid change in complex formation (see Discussion).

DISCUSSION

Elucidation of the energetics and dynamics of human pol β interactions with ssDNA is of fundamental importance for understanding the enzyme activity at the molecular level. Equilibrium studies already showed that the binding of human pol β to ssDNA is a complex process (*20*). The enzyme forms two binding modes, the (pol β)$_{16}$ and (pol β)$_5$ binding modes which differ by the number of occluded nucleotide residues in the complex with the protein (*20*). Moreover, the structural domains of the enzyme are involved differently in interactions with the nucleic acid. While both

Scheme 3

$$\text{Human pol } \beta + \text{ssDNA} \underset{k_{-D}}{\overset{k_D}{\Leftrightarrow}} E \underset{k'_{-1}}{\overset{k'_1}{\Leftrightarrow}} (P_{16}-\text{ssDNA})_1 \underset{k_{-2}}{\overset{k_2}{\Leftrightarrow}} (P_{16}-\text{ssDNA})_2 \underset{k_{-3}}{\overset{k_3}{\Leftrightarrow}} (P_{16}-\text{ssDNA})_3 \underset{k_{-4}}{\overset{k_4}{\Leftrightarrow}} (P_{16}-\text{ssDNA})_4$$

the 8- and 31-kDa domains are engaged in interactions with the ssDNA in the (pol β)$_{16}$ binding mode, only the 8-kDa domain interacts directly with the nucleic acid in the (pol β)$_5$ binding mode (*20*). We have previously determined that binding of human pol β to ssDNA oligomers is not affected by any detectable "end effects" affecting the formation of the binding modes (*19*−*23*). Therefore, the dynamics of the polymerase interactions with the nucleic acid have been addressed, using the stopped-flow technique, with the ssDNA 20-mer, which at low enzyme concentrations binds human pol β exclusively in the (pol β)$_{16}$ binding mode, and with the ssDNA 10-mer, which can only form the (pol β)$_5$ binding mode with the enzyme.

In our studies, we utilized the fact that the binding of a ssDNA, containing a fluorescein residue in place of one of the bases, to human pol β is accompanied by a significant nucleic acid fluorescence increase. The large signal change upon forming a complex with the protein is necessary to obtain the resolution required to quantitatively assess the complex mechanism of human pol β−ssDNA interactions. This is particularly important when there are several steps in the examined reaction, the amplitudes of some relaxation processes are small, and some of the relaxation times cannot be determined from the experiment. In this context, the DNA substrates, with a base substituted by fluorescein, may be very useful in the examination of other protein−nucleic acid systems where complex mechanisms require high resolutions to extract kinetic and spectroscopic parameters.

Amplitude Analysis Using the Matrix Projection Operator Technique. Relaxation times and amplitudes are two independent sets of data obtained in spectroscopic, chemical relaxation experiments. Both sets of data can provide information necessary to establish the correct mechanism of the studied reaction. Although, usually, only the relaxation times are used to obtain rate constants, the independent amplitude analysis can confirm or disprove the assumed mechanism. Also, amplitude analysis is the only direct source of information about the structure of the intermediates (*24*, *25*, *37*). Often the shortest relaxation time cannot be determined from stopped-flow data. Such a situation occurs in the case of human pol β−ssDNA complex formation analyzed in this work. However, the amplitude of this normal mode, which contains the same information as the relaxation time, can be obtained by using the fact that the total amplitude of the reaction available from the data is a simple, algebraic sum of all amplitudes of the reaction (eqs 18 and 19). The obtained amplitude of the first normal mode becomes an invaluable source of information about the rate constants and the structure of the intermediates involved in the first step of the reaction (see above).

The kinetic data are often examined by purely numerical approaches. Such analyses, although powerful in addressing the mechanism, provide limited insight into the physical nature of the intermediates of the studied reaction. In this context, the matrix projection operator technique, applied in this work, offers an experimenter closed-form expressions for the amplitudes of a complex, multistep, kinetic mechanism which require very limited numerical calculations (*24*, *25*). Moreover, the analysis of the experimentally obtained amplitudes enables the determination of spectroscopic properties of all identified intermediates, thus providing information about the structure of the intermediates, invaluable in assessing the mechanism of the reaction and unavailable by any other method.

Formation of the (Pol β)$_{16}$ Binding Mode by Human Pol β Is Described by a Multiple-Step Sequential Kinetic Mechanism. The results obtained in this work indicate that the mechanism of (pol β)$_{16}$ binding mode formation with dT(pT)$_8$-pFlu-(pT)$_{10}$ is a minimum four-step, sequential process described by Scheme 1. Thus, the enzyme−ssDNA complex undergoes three conformational transitions following the initial complex formation. The same mechanism of (pol β)$_{16}$ binding mode formation has been observed with the ssDNA thymine oligomer, dT(pT)$_{14}$-pFlu-(pT)$_4$, having the fluorescein residue located in a different part of the nucleic acid (Table 1). Therefore, the observed mechanism is not affected by the location of the fluorescent label, and it is an intrinsic property of the system. The bimolecular step is characterized by the high rate constant $k_1 = (1.8 \pm 0.3) \times 10^9$ M^{-1} s^{-1} (Table 1). However, this value must include a statistical factor of ~5 resulting from the fact that the site-size of the (pol β)$_{16}$ binding mode is only 16 ± 2 nucleotide residues (*20*). Thus, the intrinsic association rate constant is $\sim 4 \times 10^8$ M^{-1} s^{-1}. This is still a very high value, similar to the values of other very fast protein−nucleic acid recognition reactions including aminoacyl-tRNA synthetases and ribosomal proteins (*41*−*43*).

Using the Smoluchowski equation, one can estimate the theoretical value of the maximum rate constant, k_D, for the diffusion-controlled association (*44*, *45*). In our buffer conditions, this estimate is $k_D \sim 1 \times 10^{10}$ M^{-1} s^{-1} (*24*, *25*). This value indicates that the obtained bimolecular rate constant, k_1, for the formation of the (pol β)$_{16}$ binding mode is close to the diffusion-controlled value. However, additional information about the nature of the first intermediate comes from the amplitude analysis which shows that the largest increase of the nucleic acid fluorescence in the complex with the polymerase (suggesting a significant conformational change) occurs in the formation of (P$_{16}$-ssDNA)$_1$ (Table 1). Such conformational changes cannot take place in a simple collision complex, even if they are only local changes around the label, because then it would not be a collision complex (*44*). Therefore, Scheme 1 should be enlarged by an extra step, following the collision complex, E, as described by Scheme 3.

Here, k_D and k_{-D} are rate constants for the formation and dissociation of the collision complex, E, and k'_1 and k'_{-1} are the rate constants for the transition from the collision complex to (P$_{16}$-ssDNA)$_1$. The observed, apparent bimolecular rate constant k_1 is then approximately $K_D k'_1$, where $K_D = k_D/k_{-D}$.

Although the General, Kinetic Mechanisms of (Pol β)$_{16}$ and (Pol β)$_5$ Binding Mode Formations by Human Pol β Are the Same, the Nature of the Intermediates Is Different.

The analysis of the kinetic data indicates that the formation of the (pol β)$_5$ binding mode is described by the same sequential mechanism as observed for the (pol β)$_{16}$ binding mode (Scheme 2). The fact that similar steps are observed in the case of both binding modes provides the first indication that the interactions at the interface between the 8-kDa domain and the nucleic acid are dominant factors in the formation of all intermediates (see below). Although the general mechanisms are the same, there are significant differences in the nature of the formed intermediates. Such differences point out the specific roles played by the DNA-binding subsites, located on the 8- and 31-kDa domains, in the formation of both binding modes. This is already evident in formation of the (P_5-ssDNA)$_1$ and (P_5-ssDNA)$_1$ intermediates.

The bimolecular rate constants are very similar in both binding modes (Table 1). On the other hand, the dissociation rate constant k_{-1} of the (pol β)$_5$ binding mode is by a factor of ~8 higher than the value obtained in the (pol β)$_{16}$ binding mode. These data indicate that there is a much higher probability of human pol β to be released back into the solution from the (P_5-ssDNA)$_1$ intermediate in the (pol β)$_5$ binding mode than from the (P_{16}-ssDNA)$_1$ intermediate in the (pol β)$_{16}$ binding mode. The very similar values of k_1 in both binding modes and a much higher value of the dissociation rate constant k_{-1} in the (pol β)$_5$ binding mode result in an ~1 order of magnitude lower partial equilibrium constant K_1 characterizing the formation of (P_5-ssDNA)$_1$, as compared to the formation of (P_{16}-ssDNA)$_1$ (Table 1). Also, the amplitude analysis indicates that the transition to the first intermediate (P_5-ssDNA)$_1$ is not associated with a dominant fluorescence change as observed in the case of (P_{16}-ssDNA)$_1$. Thus, contrary to the (pol β)$_{16}$ binding mode, the formation of (P_5-ssDNA)$_1$ is not associated with a large nucleic acid conformational change. Recall, equilibrium studies have shown that in the (pol β)$_{16}$ binding mode both the 8- and 31 kDa domains are engaged in interactions with the ssDNA, while only the 8-kDa domain interacts with the nucleic acid in the (pol β)$_5$ binding mode (*19*). The simplest explanation of the dynamic behavior is that, in both binding modes, the association reaction (k_1) occurs through the DNA-binding subsite of the 8-kDa domain of the protein. However, in the (pol β)$_{16}$ binding mode, fast engagement of the DNA-binding subsite on the 31-kDa domain in interactions with the DNA leads to a lower value of k_{-1} of (P_{16}-ssDNA)$_1$ and to more pronounced conformational changes of the nucleic acid. In the (pol β)$_5$ binding mode, only the 8-kDa domain is involved in the formation of (P_5-ssDNA)$_1$, without the additional engagement of the 31-kDa domain. The energetics of the subsequent partial reactions in both binding modes support this conclusion.

The (Pol β)$_{16}$ and (Pol β)$_5$ Binding Modes Differ in the Energetics of the Partial Reactions. Initiating Role of the 8-kDa Domain and Stabilizing Role of the 31-kDa Domain. The first binding step generates a predominant part of the total free energy $\Delta G°$ of binding in both binding modes (Table 1). However, as we discussed above, the much higher value of K_1, characterizing the formation of (P_{16}-ssDNA)$_1$ as compared to (P_5-ssDNA)$_1$, strongly indicates that additional interacting areas are involved in the formation of (P_{16}-ssDNA)$_1$. Moreover, with the exception of (P_{16}-ssDNA)$_4$, the transitions to (P_{16}-ssDNA)$_2$ and (P_{16}-ssDNA)$_3$ are accompanied by additional favorable $\Delta G°$ changes. On the other hand, all subsequent transitions to (P_5-ssDNA)$_2$, (P_5-ssDNA)$_3$, and (P_5-ssDNA)$_4$ are characterized by the negative contribution to the total free energy of binding. With the ssDNA 10-mer, human pol β predominantly interacts using its 8-kDa domain; i.e., it can only form the (pol β)$_5$ binding mode (*19*−*23*). The obtained results indicate that, in the case of this shorter ssDNA oligomer, the polymerase cannot engage in a stable complex beyond the first intermediate. In the (pol β)$_{16}$ binding mode, formed with the ssDNA 20-mer, the nucleic acid is long enough to engage in interactions with the entire total DNA-binding site of the polymerase including, the DNA-binding subsite located on the 31-kDa domain (*19*−*23*). Thus, the data indicate that the favorable free energy changes in transitions between the intermediates of the (pol β)$_{16}$ binding mode result from additional interactions between the DNA and the DNA-binding subsite located on the large 31-kDa domain.

Notice that these intermediates are also present in the case of the (pol β)$_5$ binding mode formed with the ssDNA 10-mer, indicating that they are, in fact, induced by the interactions between the 8-kDa domain and the nucleic acid, although the 10-mer is not long enough to stabilize them through interactions with the DNA-binding subsite of the 31-kDa domain. In other words, the data suggest that the favorable energy changes in the partial steps of (pol β)$_{16}$ binding mode formation reflect efficient docking of the nucleic acid in both DNA-binding subsites of the total DNA-binding site of human pol β, following the initial association through the 8-kDa domain. In this context, the observed different stability of the (pol β)$_5$ binding mode intermediates would reflect a lack of the extra interaction areas in the DNA-binding subsite of the 31-kDa domain.

Schematic models of human pol β binding to the ssDNA in the (pol β)$_{16}$ and (pol β)$_5$ binding modes, based on thermodynamic and kinetic data, are shown in Figure 12A,B. The initial association of the enzyme with the nucleic acid in both binding modes occurs through the small 8-kDa domain. Interactions between the DNA and the polymerase at the interface of the 8-kDa domain induce conformational transitions of the nucleic acid−enzyme complex. In the case of the short ssDNA oligomer, the stability of these conformational states (intermediates) is solely based on the free energy generated through interactions with the 8-kDa domain (Figure 12B). However, in the case of the (pol β)$_{16}$ binding mode, i.e., when the ssDNA is long enough to engage the total DNA-binding site of the polymerase, the formed intermediates are additionally stabilized through interactions with the DNA-binding subsite located on the large 31-kDa domain of the enzyme (Figure 12A).

It should be pointed out that neither the (pol β)$_{16}$ nor the (pol β)$_5$ binding mode forms stable intermediates, (P_{16}-ssDNA)$_4$ and (P_5-ssDNA)$_4$. The fact that the intermediate is present in both binding modes indicates that it is generated through interactions with the 8-kDa domain. Notice that this intermediate is not even detectable in the (pol β)$_{16}$ binding mode formed with dA(pA)$_8$-pFlu-(pA)$_{10}$ (see above). Recent studies of interactions of the isolated 8-kDa domain of the analogous rat pol β showed that the domain has a much lower affinity for adenosine than for thymine homopolymers (*21*). Similar lower affinity of the intact human pol β for dA-(pA)$_8$-pFlu-(pA)$_{10}$, as compared to the thymine 20-mer, has been obtained in this work (see above). Our previous analyses

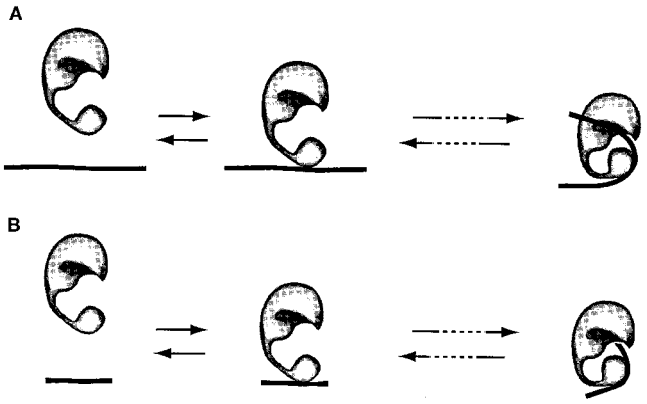

FIGURE 12: Schematic models of human pol β binding to the ssDNA in the (pol β)$_{16}$ and (pol β)$_5$ binding modes, based on the thermodynamic and kinetic data obtained in this work. In both binding modes, the enzyme initially binds the nucleic acid through the small 8-kDa domain. Several conformational transitions of the nucleic acid−enzyme complex are induced at the interface of the 8-kDa domain and the nucleic acid. In the case of the (pol β)$_{16}$ binding mode, i.e., when the ssDNA is long enough to engage the total DNA-binding site of the polymerase, the formed intermediates are additionally stabilized through interactions with the DNA-binding subsite, located on the large 31-kDa domain of the enzyme, resulting in the final equilibrium complex with both DNA-binding subsites involved in interactions with the nucleic acid (A). In the case of the short ssDNA oligomer, the stability of all conformational states and the final equilibrium complex is based solely on the free energy generated through interactions with the 8-kDa domain, without the involvement of the DNA-binding subsite of the 31-kDa domain (B) (details in text).

indicated that the formation of the (pol β)$_{16}$ and (pol β)$_5$ binding modes induces separation and immobilization of the nucleic acid bases in the complex with the protein (*19*−*23*). Also, the crystal structure of the enzyme co-complex with the DNA substrate indicates significant distortion of the nucleic acid structure in the complex (*16*). Lower macroscopic binding constants for the dA(pA)$_8$-pFlu-(pA)$_{10}$ and the less energetically favorable transitions between the intermediates, or even the absence of the intermediates, most probably reflect the fact that the adenosine oligomer has stronger base−base stacking interactions and a much less flexible structure. These properties would make any conformational adjustment of the adenosine oligomer in the complex with the protein more difficult than in the case of the thymine oligomer, as experimentally observed. Besides, significantly weaker interactions between the 8-kDa domain and dA(pA)$_8$-pFlu-(pA)$_{10}$ may not be capable of inducing the transition to (P$_{16}$-ssDNA)$_4$.

Equilibrium studies have clearly shown that specific binding of Mg^{2+} cations to the isolated rat pol β 8-kDa domain dramatically affects the domain interactions with the ssDNA by the changing the site-size of the domain−DNA complex (*21*). In the presence of magnesium, the site-size decreases from 13 ± 0.7 to 9 ± 0.6 nucleotide residues occluded by the protein (*21*). Although such data are not available for the isolated 8-kDa domain of the human enzyme, the results obtained in this work indicate that magnesium cations have a complex and not fully understood effect on interactions of human pol β in both binding modes. The significant decrease of the partial equilibrium constant K_1 characterizing the formation of (P$_5$-ssDNA)$_1$, as a result of the decreased association rate constant k_1, is not accompanied by any significant changes in partial equilibrium constants which characterize the subsequent steps in the formation of the (pol β)$_5$ binding mode (Table 2). The effect on the formation of the (pol β)$_{16}$ binding mode is different. The value of K_1 is only slightly decreased, K_2 is unaffected, K_3 is increased, but K_4 is strongly decreased in the presence of Mg^{2+}. These results would suggest a complex interplay where magnesium binding to the 8-kDa domain could control the affinities of both DNA-binding subsites of the enzyme. The effect of magnesium on the binding kinetics of the isolated 8-kDa domain of human pol β to ssDNA is currently being examined in our laboratory.

Sequential Character of the Mechanism of Human Pol β Binding to ssDNA in the (Pol β)$_{16}$ and (Pol β)$_5$ Binding Modes Excludes Preequilibrium Conformational Transition of the Enzyme Structure. Examination of the kinetics of ligand binding is a very sensitive method to detect preequilibrium, conformational transitions of the macromolecule (*24*, *25*, *37*). For instance, if human pol β existed in solution as the equilibrium of two conformational states, prior to ssDNA binding, and both states could bind the nucleic acid, then we should detect two relaxation times corresponding to the bimolecular binding steps to each conformation (*37*). The possibility of the presence of two conformations of the enzyme in solution is borne from crystallographic studies indicating that human pol β exists in an "open" conformation, and transforms into the "closed" conformation in the complex with the nucleic acid (*17*). On the other hand, both the relaxation times and amplitudes show behavior that is typical for the sequential mechanism of binding. In other words, the sequential mechanism of the formation of both, (pol β)$_{16}$ and (pol β)$_5$, binding modes provides strong evidence that the "closed" conformation of the polymerase in the complex with the DNA is induced by nucleic acid binding. Moreover, the data and analyses discussed in this work indicate that the conformational changes in human pol β are predominantly induced by the interactions between the nucleic acid and the 8-kDa domain of the protein.

ACKNOWLEDGMENT

We thank Gloria Drennan Davis for her help in preparing the manuscript.

REFERENCES

1. Hubscher, U., Nasheuer, H.-P., and Syvaoja, J. E. (2000) *Trends Biochem. Sci. 25*, 143−147.
2. Friedberg, E. C., Walker, G. C., and Siede, W. (1995) *DNA Repair and Mutagenesis*, ASM Press, Washington, DC.
3. Budd, M. E., and Campbell, J. L. (1997) *Mutat. Res. 384*, 157−167.
4. Fry, M., and Loeb, L. A. (1986) *Animal Cell DNA Polymerases*, CRC Press, Inc., Boca Raton, FL.
5. Johnson, R. E., Prakash, S., and Prakash, L. (1999) *Science 283*, 1001−1004.
6. Sobol, R. W., Horton, J. K., Kühn, R., Hua, G., Singhal, R. K., Prasad, R., Rajewsky, K., and Wilson, S. H. (1996) *Nature 379*, 183−186.
7. Wiebauer, K., and Jiricny, J. (1990) *Proc. Natl. Acad. Sci. U.S.A. 87*, 5842−5845.
8. Masumoto, Y., and Kim, K. (1995) *Science 269*, 699−702.
9. Hoffman, J. S., Pillaire, M. J., Maga, G., Podust, V., Hubscher, U., and Villani, G. (1995) *Proc. Natl. Acad. Sci. U.S.A. 92*, 5356−5360.
10. Matsumoto, Y., and Bogenhagen, D. F. (1989) *Mol. Cell. Biol. 9*, 3750−3757.

11. Matsumoto, Y., and Bogenhagen, D. F. (1991) *Mol. Cell. Biol. 11*, 4441−4447.
12. Matsumoto, Y., Kim, K., and Bogenhagen, D. F. (1994) *Mol. Cell. Biol. 14*, 6187−6197.
13. Singhal, R. K., Prasad, R., and Wilson, S. H. (1995) *J. Biol. Chem. 270*, 949−957.
14. Hammond, R. A., McClung, J. K., and Miller, M. R. (1990) *Biochemistry 29*, 286−291.
15. Pelletier, H., Sawaya, M. R., Kumar, A., Wilson, S. H., and Kraut, J. (1994) *Science 264*, 1891−1903.
16. Pelletier, H., Sawaya, M. R., Wolfle, W., Wilson, S. H., and Kraut, J. (1996) *Biochemistry 35*, 12762−12777.
17. Sawaya, M. R., Pelletier, H., Kumar, A., Wilson, S. H., and Kraut, J. (1994) *Science 264*, 1930−1935.
18. Joyce, C. M., and Steitz, T. A. (1994) *Annu. Rev. Biochem. 63*, 777−822.
19. Rajendran, S., Jezewska, M. J., and Bujalowski, W. (1998) *J. Biol. Chem. 273*, 31021−31031.
20. Jezewska, M. J., Rajendran, S., and Bujalowski, W. (1998) *J. Mol. Biol. 284*, 1113−1131.
21. Jezewska, M. J., Rajendran, S., and Bujalowski, W. (2001) *Biochemistry 40*, 3295−3307.
22. Jezewska, M. J., Rajendran, S., and Bujalowski, W. (2001) *J. Biol. Chem. 276*, 16123−16136.
23. Rajendran, S., Jezewska, M. J., and Bujalowski, W. (2001) *J. Mol. Biol. 308*, 477−500.
24. Bujalowski, W., and Jezewska, M. J. (2000) *J. Mol. Biol. 295*, 831−852.
25. Bujalowski, W., and Jezewska, M. J. (2000) *Biochemistry 39*, 2106−2122.
26. Rajendran, S., Jezewska, M. J., and Bujalowski, W. (2000) *J. Mol. Biol. 303*, 773−795.
27. Abbotts, J., SenGupta, D. N., Zmudzka, B., Widen, S. G., Notario, V., and Wilson, S. H. (1988) *Biochemistry 27*, 901−909.
28. Edelhoch, H. (1967) *Biochemistry 6*, 1948−1954.
29. Gill, S. C., and von Hippel, P. H. (1989) *Anal. Biochem. 182*, 319−326.
30. Jezewska, M. J., and Bujalowski W. (1996) *J. Biol. Chem. 271*, 4261−4265.
31. Jezewska, M. J., Rajendran, S., Bujalowska, D., and Bujalowski, W. (1998) *J. Biol. Chem. 273*, 10515−10529.
32. Jezewska, M. J., Rajendran, S., and Bujalowski, W. (1998) *J. Biol. Chem. 273*, 9058−9069.
33. Jezewska, M. J., Rajendran, S., and Bujalowski, W. (1997) *Biochemistry 37*, 3116−3136.
34. Bujalowski, W., and Jezewska M. J. (2000) *Spectrophotometry & Spectrofluorimetry. A Practical Approach* (Gore, M. G., Ed.) Chapter 5, Oxford University Press, Oxford, U.K.
35. Bujalowski, W., Greaser, E., McLaughlin, L. W., and Porschke, D. (1986) *Biochemistry 25*, 6365−6371.
36. Bujalowski, W., Jung, M., McLaughlin, L. W., and Porschke, D. (1986) *Biochemistry 25*, 6372−6378.
37. Bernasconi, C. F. (1976) *Relaxation Kinetics*, Academic Press, New York.
38. Pilar, F. L. (1968) *Elementary Quantum Chemistry*, Chapter 9, McGraw-Hill, New York.
39. Saenger, W. (1984) *Principles of Nucleic Acid Structure*, Chapter 13.
40. Porschke, D. (1976) *Biochemistry 15*, 1495−1499.
41. Mulsch, A., Colpan, M., Wollny, E., Gassen, H. G., and Riesner, D. (1981) *Nucleic Acids Res. 9*, 2367−2385.
42. Riesner, D., Pingoud, A., Boehme, D., Peters, F., and Mass, G. (1976) *Eur. J. Biochem. 68*, 71−80.
43. Krauss, G., Riesner, D., and Maass, G. (1976) *Eur. J. Biochem. 68*, 81−93.
44. Connors, K. A. (1990) *Chemical Kinetics. The Study of Reaction Rates in Solution*, Chapter 4, VCH, New York.
45. Berry, R. S., Rice, S. A., and Ross, J. (1980) *Physical Chemistry*, Chapter 15, John Wiley & Sons, New York.

BI011173J